2014

Modeling of an upper Midwest forest boundary layer and vehicle indoor air quality

Phillip Stratton

Modeling of an Upper Midwest Forest Boundary Layer and Vehicle Indoor Air Quality

by

Phillip Stratton

Thesis

Submitted to the Department of Chemistry

Eastern Michigan University

in partial fulfillment of the requirements

for the degree of

MASTER OF SCIENCE

in

Chemistry

Thesis Committee:

Gavin Edwards, Ph.D, Chair

Heather Holmes, Ph.D.

Andrew Ross, Ph.D.

June 16, 2014

Ypsilanti, Michigan

Acknowledgements

I cannot express enough thanks to Dr. Gavin Edwards, my committee chair, for his continued support and encouragement along with Dr. Heather Holmes and Dr. Andrew Ross, also on my committee. I would also like to thank Dr. Hedeel Evans for her support academically and as a mentor. I offer my sincere appreciation for the learning opportunities provided by my committee and course professors. Though the preparation of this manuscript was overshadowed by a divorce, an internship with NASA, the passing of family, and multiple computer failures, I was able to complete this work with the support of my classmates and friends. Thanks to my parents as well, Mr. Cliff Stratton and Mrs. Dawn Viau, for their unconditional love and support, without which I would not have developed into the person I am today.

Abstract

The key to understanding tropospheric chemistry begins with the hydroxyl and hydroperoxy radicals. Recent research suggests that there is still considerable uncertainty in our understanding of the sources of these radicals and their role as sinks. The work detailed in this thesis describes a computational approach to modeling the hydroxyl and hydroperoxy radicals in a forest environment and attempts to shed further light on the radical budget in a typical Northern Hardwood forest. Additionally, research was conducted with United States Council for Automotive Research in collaboration with Ford, General Motors, and Chrysler to develop a global standard for vehicle indoor air quality test methodologies. An initial evaluation of materials to validate test and analysis process has been completed. In addition to establishing the identity of a material for an internal standard, a VOC specific emission algorithm to predict cabin VOC concentrations for a given set of control parameters was established.

Table of Contents

List of Tables

List of Figures

Climate

Earth is a planet that consists of several different biologically and geologically diverse regions. This diversity generates the weather observed throughout the world. These weather patterns allow a distribution and equalization of the energy (radiation) entering and leaving the atmosphere. Earth does not receive radiation evenly across its surface as a result of the atmosphere surrounding the planet and the obliquity, the angle between an object's rotational axis and its orbital axis, of Earth. The obliquity results in the equator receiving more solar radiation and the poles receiving significantly less radiation. As the energy absorbed near the equator is radiated towards the colder polar regions or radiated back into space in an attempt to equalize energy differences, energy is transported around the world through differing air masses and ocean currents.

Clouds also play an important role in the distribution of energy around the globe. Some clouds reflect radiation (approximately 20%) back to space while others sequester energy and keep it close to the surface (Seinfeld and Pandis, 2006). Low-level, white clouds reflect radiation effectively cooling the planet. High, connective clouds have a net warming effect on the planet. These clouds absorb longer wavelength radiation emitted from the earth and re-direct back to Earth.

Atmospheric Layers

Through the end of the 19th century it was believed that atmospheric temperature would decrease to absolute zero with increasing altitude. In 1896, Léon Philippe Teisserenc de Bort sent atmospheric balloons equipped with temperature measuring equipment and proved this not to be the case (Fonton). The data obtained showed the temperature actually stopped falling around 11 km, and remained constant. This led to the understanding that the atmosphere is divided into four

distinct regions based on temperature. Figure 1 illustrates the United States Standard Atmosphere model. The U.S. Committee on Extension to the Standard Atmosphere (COESA) in collaboration with National Oceanic and Atmospheric Administration (NOAA) published several versions of the U.S. Standard Atmosphere model, with the 1976 version being the most recent. The U.S. Standard Atmosphere model divides the atmosphere into layers with linear temperature distributions. The other values are computed from basic physical constants and relationships.

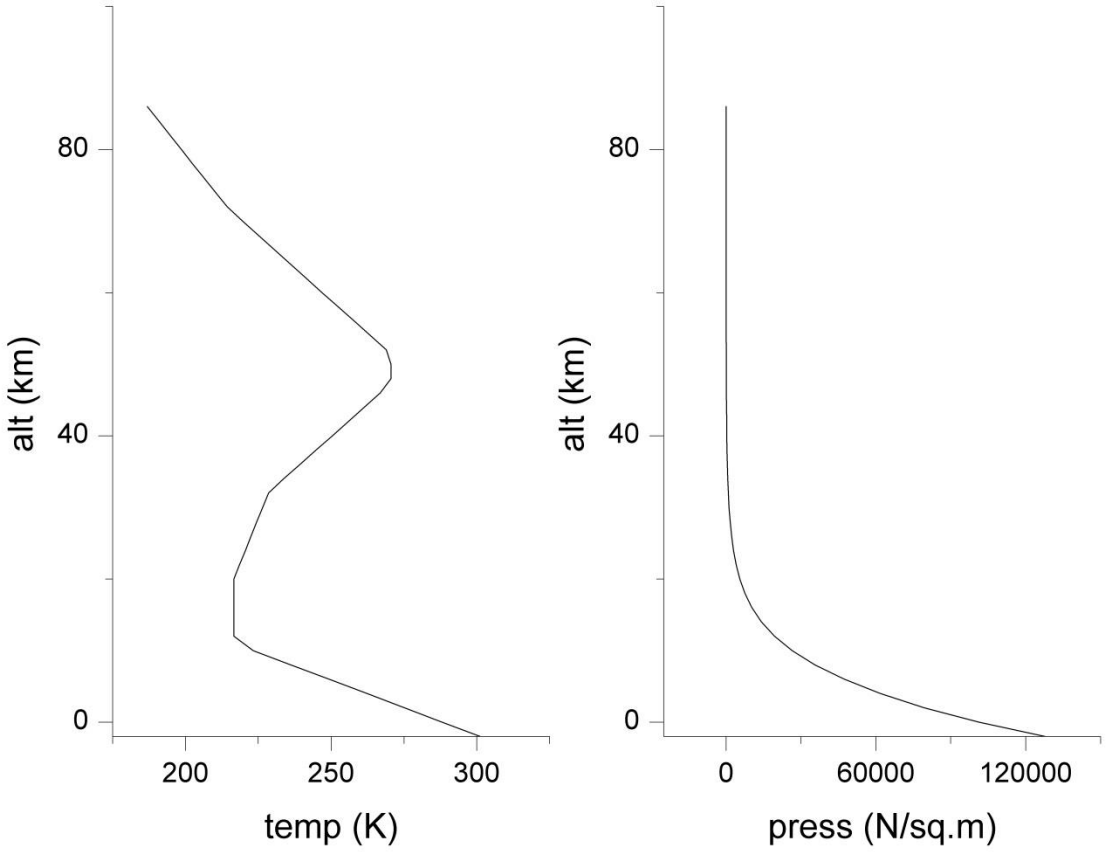

Figure 1: Comparison of an International Standard Atmosphere graph of geometric altitude against temperature and pressure

The troposphere is the lowest region in the atmosphere, characterized by decreasing temperature with increasing altitude. The troposphere contributes minimally to the total height of the atmosphere, though it contains approximately 90% of the total mass of the atmosphere. At the lowest level of the troposphere is found the biosphere or the part of the atmosphere that contains all living things. Depending on latitude, the "tropopause" is observed between 10-15 km altitudes. The tropopause as defined by the World Meteorological Organization (WMO) is the lowest altitude where the temperature lapse rate, that is the rate of temperature decrease with altitude, drops to 2 K km^{-1} or less. The average lapse rate does not exceed 2 K km^{-1} within the next 2 km (Holton et al., 1995). Just above the tropopause is the stratosphere which continues up to an altitude of 45-55 km to the stratopause. The stratosphere is characterized by a temperature that increases with raising altitude, which is due to the exothermic production and destruction of ozone in addition to the adsorption of radiation (Chapman, 1930). Above the stratopause is the mesosphere, which is characterized by a decrease in temperature with increasing altitude, continuing to an altitude of approximately 80-90 km altitude. The thermosphere is found above the mesopause continuing to approximately 500 km, with an increase in temperature with an increase in altitude. The rise in temperature with altitude is a result of absorption of UV radiation by N_2 and O_2. Above the thermosphere is the exosphere where gas molecules that retain enough energy can escape Earth's gravitational field. The work described within this thesis will focus on the interaction and chemistries of the biosphere and the troposphere.

Scale of Atmospheric Processes

The atmosphere can be thought of as a chemical reactor with continuous injection, production, removal, and destruction of chemical species. The lifetime of a species is defined as the average time a molecule remains in a given area. The lifetime of a species is calculated by

dividing the mass of the species in the area and dividing it by the sum of the out flow, and the loss due to chemical reactions and deposition. Gases may have lifetimes ranging from seconds to greater than 50,000 years (Atkinson, 1987; Ravishankara et al., 1993).

Chemical Transformation

Chemical species in the atmosphere have an overwhelming propensity to interact and take part in various chemical reactions. These interactions can change the original species not only chemically, but physically as well. The species is most often transformed into a higher oxidative state variant of the original species (Seinfeld and Pandis, 2006). Along with a change in oxidative state, these species can undergo transformation into various species with completely different chemical properties. These properties may increase the reactivity of the parent species or render them inert. A simple example of this can be seen in the well-studied formation of acid rain. For example, sulfur dioxide is converted into sulfuric acid, which is extremely water soluble and will associate with water molecules almost instantly.

$$SO_2 + OH + M \rightarrow HOSO_2 + M \quad \text{(Reaction 1)}$$

$$HOSO_2 + O_2 \rightarrow HO_2 + SO_3 \quad \text{(Reaction 2)}$$

$$SO_3 + H_2O + M \rightarrow H_2SO_4 + M \quad \text{(Reaction 3)}$$

Atmospheric Composition

About 78% of the atmosphere is molecular nitrogen, 21% of the atmosphere is molecular oxygen, with the remaining 1% consists of water vapor, noble gases, and other trace gases. These trace gases play a crucial role in the chemical properties and radiative state of the atmosphere. Molecular nitrogen is inherently stable as a result of the triple bond and O_2 is only slightly less inert, leaving 1% of trace gases to influence tropospheric chemistry. Trace gases will have

differing influences on the chemistries of the atmosphere as their lifetimes (when a species is lost through chemical processes) and residence times (when a species is lost through a physical process) can be substantially different.

Trace Constituents

Although a complete listing of the trace gases observed is beyond the scope of this work, the general reactions of various groups of compounds are described here.

A class of inorganic gases in the atmosphere is the sulfur containing compounds. Hydrogen sulfide (H_2S), carbonyl sulfide (COS), sulfur dioxide (SO_2), and dimethyl sulfide (DMS, $(CH_3)_2S$) are some of the common atmospheric sulfur containing gases found in the atmosphere. The reactivity of this class of compounds is inversely proportional to their oxidation state. As their oxidation state increases, their water solubility increases. Sulfur containing compounds tend to have very short resident times. Low oxidation state compounds have a high reactivity and high oxidation state compounds have increased water solubility.

A second class of inorganic gases found in the atmosphere is the nitrogen containing compounds. The oxides of nitrogen NO and NO_2, (referred to from this point forward as NO_x), are important to the overall oxidation rate and ozone distribution in the troposphere. NO_x molecules compete with other VOC molecules to react with the hydroxyl radical, OH, the primary tropospheric oxidant (see later). Ozone production sensitivity in regards to the NO_x-VOC ratio is difficult to predict. Ozone-precursor sensitivity predictions are generally derived from 3-dimensional Eulerian chemistry or transport models. Different assumptions in models may lead to very different results for predicted sensitivity to NOx and VOC. Kirchner et al. (2001) have identified three regimes of ozone production based on box models. These regimes help predict ozone concentrations. The sum of the products of the atmospheric oxidation of NO_x

and NO_x concentration are known as reactive nitrogen, denoted NO_y. Included in this reactive nitrogen category is nitrous acid (HONO), nitrate radical (NO_3), dinitrogen pentoxide (N_2O_5) nitric acid (HNO_3), alkyl nitrates ($RONO_2$), and peroxyalkyl nitrates ($ROONO_2$).

Carbonyls also play a significant role influencing the chemistry of the atmosphere, because they are responsible for the production of ozone and tropospheric radicals. This can be illustrated by looking at formaldehyde as an example. The photolysis of formaldehyde is a significant source of free radicals in the sunlit troposphere because of the longer wavelength threshold (300-340 nm) of the radical channel relative to the photolysis of O_3 (below 310 nm) in the troposphere. As can be seen in (*Reaction 4* and *(*Reaction 5, there are two pathways for the photolysis of formaldehyde. The latter dominates at longer wavelengths (Atkinson et al., 2006).

$$HCHO + h\nu \xrightarrow{1} H + HCO \quad \text{(Reaction 4)}$$

$$\xrightarrow{2} H_2 + CO \quad \text{(Reaction 5)}$$

Formaldehyde can also react with the hydroxyl radical as shown in (*Reaction 6*.

$$HCHO + OH \rightarrow HCO + H_2O \quad \text{(Reaction 6)}$$

The formyl radical (HCO) in these reactions also reacts rapidly with molecular oxygen to form hydroperoxy radicals (HO_2) and carbon monoxide. Carbonyls (e.g. formaldehyde, acetaldehyde, acetone, etc.) are produced through the oxidation of hydrocarbons or are directly emitted from vegetation (Kotzias et al., 1997).

Isoprene, 2-methyl-1,3-butadiene, is classified as an isoprenoid, and is considered one of the most important biological volatile organic compounds (BVOC) as it reacts with hydroxyl radicals, nitrate radicals, and ozone (Carter and Atkinson,1996; Paulson and Seinfeld, 1992; Paulson et al., 1992a; Paulson et al., 1992b). Isoprene is emitted from a large variety of

vegetation and appears to be a byproduct of photosynthesis, as it is only emitted in the presence of photosynthetically active radiation (PAR), from 400 and 700 nm, with emission proportional to temperature (Gunther et al., 1995). Isoprene emissions vary from plant species to plant species, and are also temperature and light dependent (Kesselmeier and Staudt,1999).

The biosynthetic pathway leading to the formation of isoprene also leads to the formation of monoterpenes and sesquiterpenes, which can be classified by the number of C_5 units present. Isoprene is classified as a hemiterpene as it has one C_5 subunit. Structures with more than one C_5 unit are classified as mono- and sesquiterpenes. This addition is potentially limitless with groups of greater than C_{45} being classified as polyterpenes. The larger terpenoids (greater than C_{15}) were not be considered within this work as they are substantially less volatile and have little influence on the chemistries of the troposphere.

The dependence of BVOC emission on plant species poses a significant obstacle to the accurate representation of biogenic emissions. A table detailing the emission of several alkane, alkene, and oxygenated species can be found in Kesselmeier and Staudt (1999). In addition to the isoprenoids, several other classes of BVOC's exist. The simplest classes are the alkanes and alkenes, of which methane, ethane, propane, and butane are the most common. The major sources of these emissions are from trees, crops, grass, and other marshlands (Zimmerman, 1979). There are also well known sources for the more reactive, ethane, propene, and butane with rates of emission being 2.63, 1.13, and 0.41×10^{10} molecules cm^{-2} s^{-1} (Goldstein et al., 1996).

Photochemistry

Actinic flux is the radiative flux, capable of inducing photochemical reactions, from all directions on a given volume of air. Actinic flux is related to but not equal to the available

radiation, or irradiance, and can be direct radiation, Raleigh or Mie scattered radiation, and even reflected radiation (Madronich, 1987). It is important to consider this differentiation when calculating rates of photodissociation as not all wavelengths that fall onto the Earth's atmosphere will penetrate to the tropopause and below.

If an incident photon has enough energy when interacting with a molecule, that molecule will undergo photodissociation. This energy can be represented by *h*ν according to Planck's law. With this it is possible to represent photochemical reactions in the following manner, where A^* is the electronically excited state of molecule A.

$$A + h\nu \rightarrow A^* \qquad \text{(Reaction 7)}$$

The molecule in this excited state can then react in one of five pathways:

Dissociation	$A^* \xrightarrow{1} B_1 + B_2$	(Reaction 8)
Direct Reaction	$A^* + B \xrightarrow{2} C_1 + C_2$	(Reaction 9)
Fluorescence	$A^* \xrightarrow{3} A + h\nu$	(Reaction 10)
Collisional Deactivation	$A^* + M \xrightarrow{4} A + M$	(Reaction 11)
Ionization	$A^* \xrightarrow{5} A^+ + e^-$	(Reaction 12)

The reaction shown in (Reaction *8*) above, and in greater detail below, is a photodissociation reaction that is prominent in atmospheric chemistry.

Photolysis

The formation of A* is related to photolysis frequency ("*j* value"), or the rate of photon absorption. This first-order rate constant for photolysis has units of s^{-1}. The *j* value for a specific process must be known in order to understand the fate of a molecule after absorption of

radiation. The elucidation of *j* values requires the knowledge of three parameters; actinic flux (F), absorption cross section (σ), and the quantum yield (φ). The absorption cross section of a molecule refers to its ability to absorb a photon or a particular energy, and is related to the mass attenuation coefficient ($\frac{\mu}{\rho}$) as shown in (Equation *1*). The value of the absorption cross section for several photochemical reactions has been well documented in research done by DeMore et al. (1997).

$$\sigma = \left(\frac{\mu}{\rho}\right) m_a / N_A \qquad \text{(Equation 1)}$$

$$\mu = (\mu/\rho)_1 \rho_1 + (\mu/\rho)_2 \rho_2 + \cdots \qquad \text{(Equation 2)}$$

The attenuation coefficient, μ, is a measure of how readily a beam is attenuated by a medium. Larger values represent faster attenuation times whereas smaller values represent a medium that the beam readily passes through. The actual attenuation coefficient is calculated via (Equation *2* where each term in the sum is the mass attenuation coefficient and density of a different component. Dividing the attenuation coefficient by the density of the chemical species gives the mass attenuation coefficient. N_A is Avogadro's number.

Just as the absorption cross section has been well studied, the quantum yield has been well studied but with differing viewpoints. The quantum yield is the ratio of the number of molecules that undergo reaction to the number of photons absorbed. It is a number between 0 (absorption of no photons) and 1 (absorption of all photons). With this information it is possible to quantitate the photolysis frequency between two wavelengths, λ_1 and λ_2, via (Equation 3.

$$j = \int_{\lambda_1}^{\lambda_2} \sigma(\lambda, T) \phi(\lambda, T) F(\lambda) d\lambda \qquad \text{(Equation 3)}$$

Equation *3* is often approximated by summing over a small wavelength interval (5 nm) utilizing midpoint or trapezoidal rules as illustrated in (Equation 4).

$$j = \sum_{i} \bar{\sigma}(\lambda_i, T)\bar{\phi}(\lambda_i, T)\bar{F}(\lambda_i) \qquad \text{(Equation 4)}$$

This is done by averaging the absorption cross section, quantum yield, and actinic flux values centered at a given wavelength, λ_i. Figure 2 represents plots, generated from raw data taken from Seinfeld and Pandis, of actinic flux, absorption cross section, quantum yield and the photolysis rate of NO_2, at noon on July, 1 at 298 K along the 40^{th} parallel (2006).

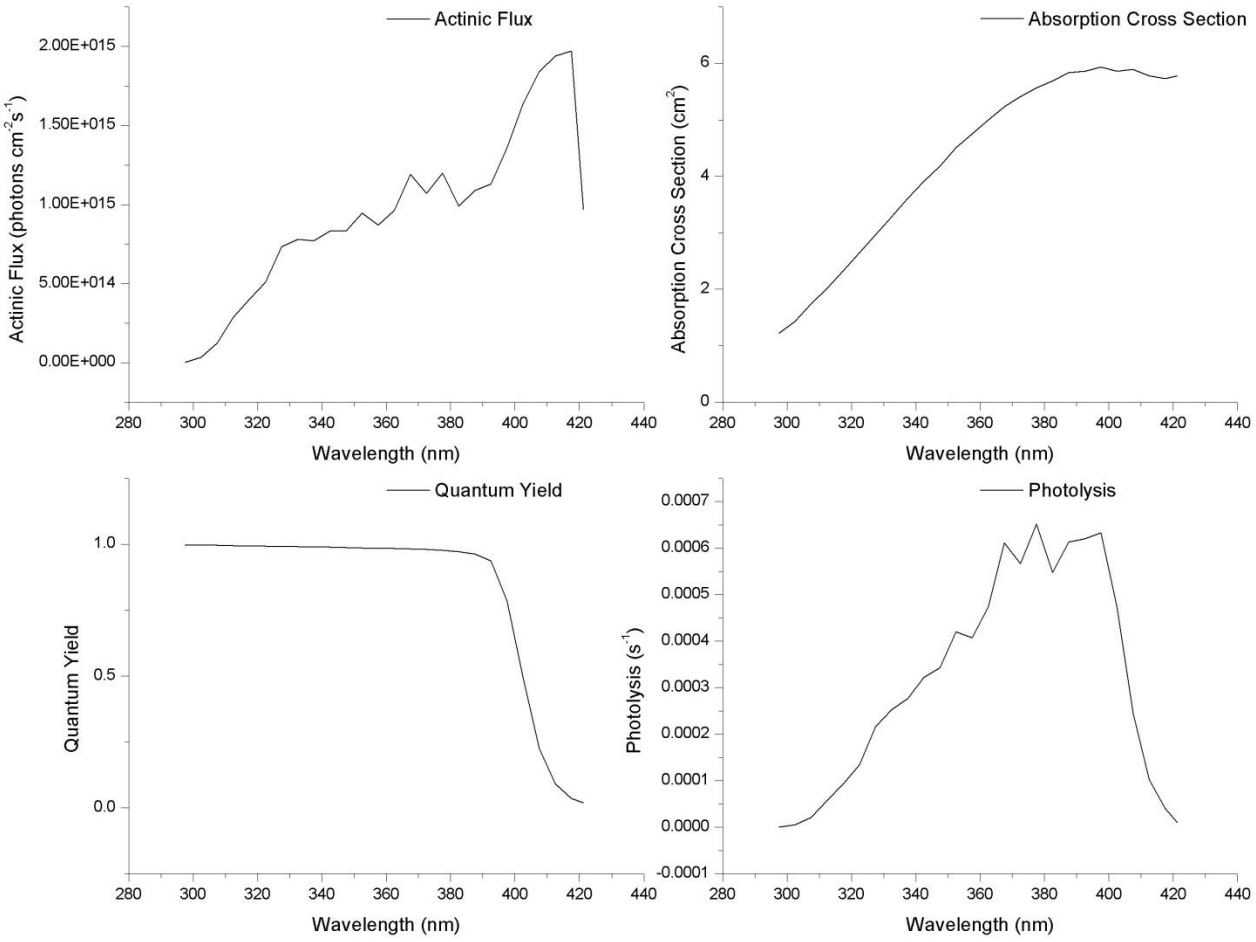

Figure 2: Change in molecular parameters with wavelength

The observed actinic flux drop-off around 410 nm is a result of the h Fraunhofer line (Hδ). Fraunhofer lines are spectral absorption lines produced whenever a cold gas is between a broad spectrum photon source and the detector. When observing the solar spectrum these Fraunhofer lines are a result of absorption by chemical elements in the atmosphere. The absorption at 410 nm is a result of the delta band (quantum number n=6 transitioning to n=2) of the Balmer series from the hydrogen atom.

Radical Chemistries

Nitrogen dioxide is one of the most important chemical species in atmospheric chemistry as it can absorb radiation over the entire visible and ultraviolet spectrum in the troposphere. The photodissociation of NO_2 (Reaction *13*) caused by the absorption of wavelengths up to about 420 nm, followed by the reaction of the ground state singlet oxygen with molecular oxygen in the presence of a quenching species (Reaction *14*) is the major source of tropospheric ozone, with minimal contributions from stratospheric transport (Logan et al., 1981;Finlayson-Pitts and Pitts,1997; Hintsa et al., 1998).

$$NO_2 + h\nu \rightarrow NO + O(^3P) \quad \text{(Reaction 13)}$$

$$O(^3P) + O_2 \xrightarrow{M} O_3 \quad \text{(Reaction 14)}$$

The formation of O(^{1}D) atoms from ozone photolysis is one of the most important chemical processes in atmospheric chemistry, since it is followed by the generation of OH radicals.

$$O_3 + h\nu \rightarrow O_2 + O(^1D) \quad \text{(Reaction 15)}$$

$$O(^1D) + H_2O \rightarrow 2\,OH \quad \text{(Reaction 16)}$$

It has been debated at what wavelength the quantum yield tended towards zero, with more recent studies suggesting that the quantum yield at wavelengths between 310 and 375nm produce significant amounts of O(^{1}D) (DeMore et al., 1997; Bauer et al., 2000). Plots of actinic flux, absorption cross section, quantum yield, and photolysis frequencies can be generated similar to that shown previously in Figure 2. Ozone formation is nearly always initiated by the reaction of OH radical with a VOC or CO as seen in reactions *17* and *(*Reaction 18). NO is then converted to

NO_2 after reacting with RO_2 or HO_2 ((Reaction 19) and *(*Reaction 20)). NO_2 is then photolyzed to O_3 as was seen in (Reaction *13*)and *(*Reaction *14*).

$$VOC + OH \overset{O_2}{\rightarrow} RO_2 + H_2O \quad \text{(Reaction 17)}$$

$$CO + OH \overset{O_2}{\rightarrow} HO_2 + CO_2 \quad \text{(Reaction 18)}$$

$$RO_2 + NO \overset{O_2}{\rightarrow} VOC' + HO_2 + NO_2 \quad \text{(Reaction 19)}$$

$$HO_2 + NO \rightarrow OH + NO_2 \quad \text{(Reaction 20)}$$

(*Reaction 13*) through *(*Reaction 16) will not necessarily lead to the production of ozone as competing reactions can act as removal pathways for ozone as well. The net production of ozone can occur in the presence of species that can oxidize NO to NO_2. Under low NO_x conditions, the cross-reactions involving RO_2 and HO_2 will lead to termination of the radicals through the formation of peroxides and other species. Under elevated levels of NO_x the RO_2 radicals will be propagated to HO_2 and then to OH through (Equation 19) and *(*Equation 20). Given the complexity of the chemistry as well as the meteorology, quantitatively linking emissions of VOCs and NO_x to the concentrations of O_3 and other photochemical oxidants and trace species at a particular location and time is not straightforward.

CABINEX Field Campaign

The University of Michigan Biological Station (UMBS) is located along the boundary of Cheboygan and Emmet Counties in the northern portion of Michigan's lower peninsula at 45°30'N, 84°42'W and 238 meters above sea level (Figure 3). This area is characterized as a "mixed" or "transition" forest, with northern hardwood, aspen, conifers, pine, red oak, and grass-

covered sand dunes along the coast (Pressley et al., 2005; Carroll et al., 2001). The Program for Research on Oxidants: PHotochemistry, Emissions and Transport, (PROPHET) is a research site that has been in operation since 1997. The PROPHET site was where data for the Community Atmosphere-Biosphere Interactions EXperiment (CABINEX) was conducted. Fifty-seven researchers from 16 universities and research institutions investigated three outstanding questions: How do BVOC emissions impact HO_x radical chemistry in the near-canopy environment? Does BVOC photochemistry in the canopy impact new particle formation or growth? What impact will changing BVOC emissions from forest succession have on HO_x and aerosol chemistry?

PROPHET has now become a well-established research site for atmospheric chemistry research with support from the National Science Foundation, the University of Michigan, Western Michigan University, and Purdue University. On site there is a 31-meter tower which can house several sampling apparatuses depending on the needs of researchers at any given time. A 34-meter pyrex sampling tube with an inner-diameter of 5 cm bring air from the top of the tower into an adjacent pole barn which is equipped as an on-site laboratory. A blower moves air through the sampling tube at about 3300 liters per minute. For species that are too reactive to transport through a manifold from the top of the tower (OH, HO_2, HNO_3, etc…) instruments can also be mounted directly to the tower. Calibration gases, pump exhaust, manifold exhaust, and heat are vented via underground piping. These potential sources of contamination is transported several hundred meters and exhausted near the site access road, which is located to the east of the measurements site. An additional UMBS research facilities utilized in this study was the AmeriFlux site, located 132 m north-northeast of the PROPHET Tower which includes a 50-meter tower from which CABINEX flux measurements are made.

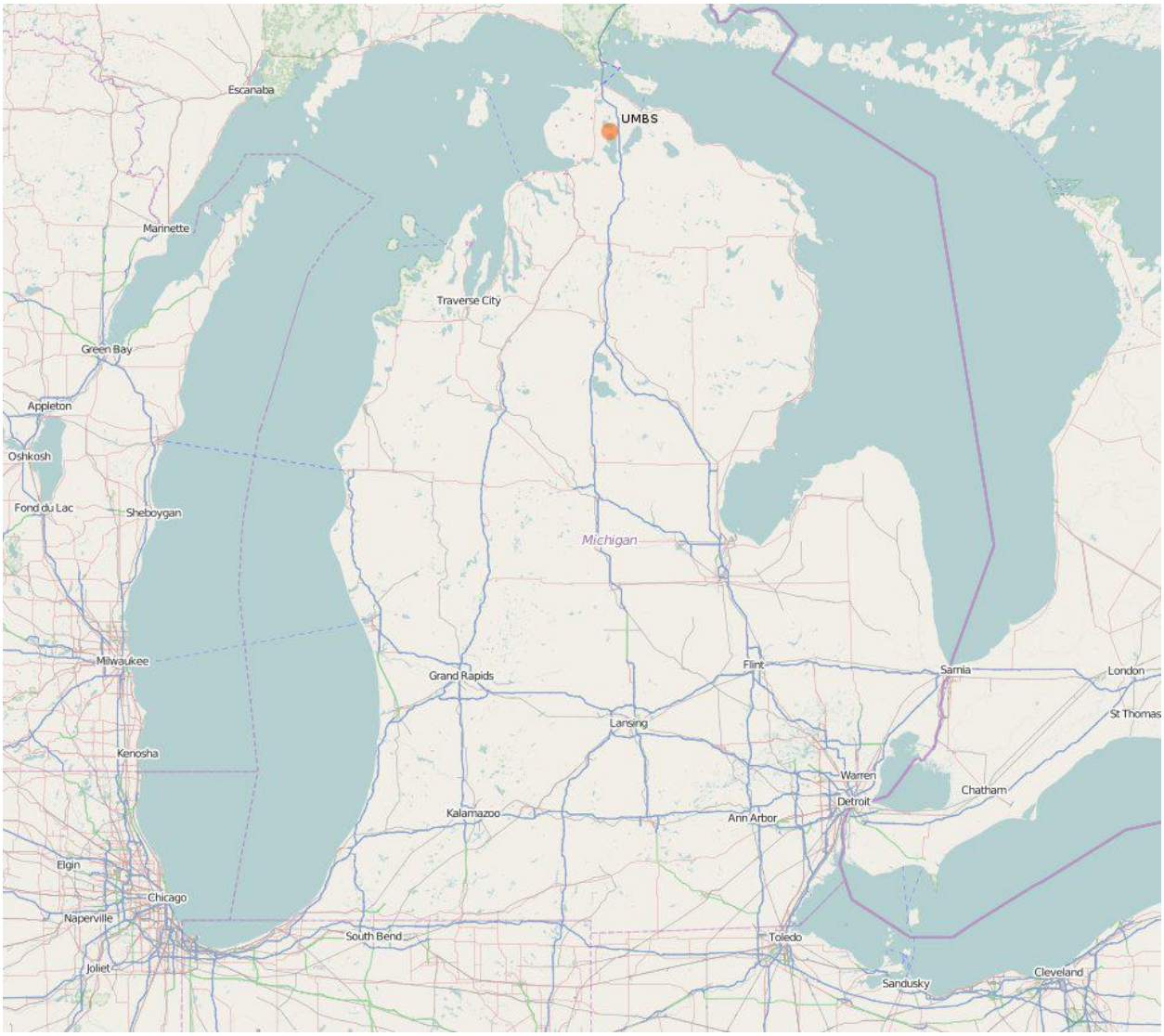

Figure 3: OpenStreetMap of Michigan with the University of Michigan Biologial Station highlighted in orange (source: http://www.openstreetmap.org).

PROPHET is located in a forested area located on University of Michigan property approximately 3.5 km west of the UMBS. This region is located about 5.5 km east of Pellston below the boreal forests resulting in temperate broadleaf and mixed forests. Pellston is located just 5.5 km to the west of the UMBS and has a population of just over 800. Air currents are of a northwesterly, westerly, or southwesterly nature with occasional northerly flow [Moody and Sampson, 1989] and so a few cities near PROPHET that may influence the air quality should be

noted. Traverse City, with a population of near 15,000, is located approximately 180 km to the southwest where the shoreline is populated with summer homes. Alpena lies about 120 km to the southeast with a population of just shy of 10,500 and a cement plant that burns construction waste as fuel for the manufacture of cement. Sault St. Marie, Michigan and Sault St. Marie, Ontario are approximately 125 km to the north with populations of near 14,200 and 75,100 respectively. Detroit is located about 350 km to the southeast with a population of 706,500 and a metropolitan area (Lapeer, Livingston, Macomb, Oakland, St. Clair, and Wayne counties) population exceeding 4,500,000 people. Still further southwest is Chicago, about 450 km, is home to 2,700,000 people, with a metropolitan area population of greater than 9,500,000 people (United States Census Bureau, 2013; Statistics Canada, 2013).

The local biomass in the vicinity of the PROPHET site is dominated by Aspen, accounting for about 90% of the isoprene-emitting biomass with the remaining 10% attributable to Northern Red Oak, resulting in an average emission rate of approximately 150 g m^{-2} (leaf area) (Westberg et al., 2012). Due to high emissions of isoprene and relatively low but highly variable NO_x concentrations, UMBS is an ideal site for studies of isoprene chemistry. Emissions inventories have long been noted for being one of the most, if not the most, uncertain aspect of air quality modeling (Sawyer et al., 2000). This uncertainty inhibits accurate air quality modeling (Hanna et al., 1998), effective air quality management, and detailed understanding of the mechanisms impacting the formation and fate of particulate matter in the atmosphere. For example, in modeling studies, the inclusion of inaccurate emissions can lead to either poor model performance or to the introduction of unforeseen, and thus not accounted for, errors being introduced (NARSTO, 2000). Understanding the formation and transport of pollutants requires knowing the properties and rates of source emissions.

Past results from PROPHET show that the local photochemistry has been controlled by isoprene (Bartket et al., 2001). As forest composition changes, the mixture of BVOC will change. Emissions of larger BVOCs, such as monoterpenes and sesquiterpenes, are of increasing importance and have the potential to contribute more at this site because of forest succession. Aspen are currently the major species in the forest and emit large amounts of isoprene. Now emerging from much of the understory are white pines that emit no isoprene but do emit monoterpenes.

PROPHET Measurements during CABINEX

Measurements made during the campaign can be seen in Table 1. The Indiana University provided HO_x measurements via laser induced fluorescence (LIF) utilizing the fluorescence assay by gas expansion (FAGE) technique (Hard et al., 1984). The instrumentation has been described in detail elsewhere (Dusanter et al., 2008, 2009a), as such only a brief summary will be provided. HO_2 is measured by converting the HO_2 to OH radical in the expansion chamber via the addition of NO (Hard et al., 1995). FAGE is capable of detecting sub-pptv levels of peroxy radicals (Amedro et al., 2012). Though the technique is not absolute in that it requires calibration to measure the instrument's sensitivity to OH radical (or HO_2), COH (or CHO_2), which is then used to later convert the measured OH radical signal into a concentration ((Equation 5). The instrument first recorded measurements at ground level, and was then moved to the top of the tower for canopy level measurements. The work presented here focuses only on the above canopy measurements.

Washington State University measured isoprene, the sum of methyl vinyl ketone and methacrolein (MVK + MACR), the sum of monoterpenes, formaldehyde, acetaldehyde, methanol, methyl hydroperoxide, acetone, toluene, benzene, and the sum of C2-alkylbenzenes

using proton-transfer reaction mass spectrometer (PTR-MS). Nitrogen oxides were also measured by Washington State University using an instrument based on chemiluminescence of NO and equipped with a blue light photolytic converter for NO_2 measurements (Air Quality Design, Inc.). The University of Michigan measured carbon monoxide with a Thermo Environmental Instruments Inc. (48C) and ozone with Thermo Environmental Instruments Inc (49C). Photolysis frequencies for NO_2, O_3, HONO, H_2O_2, HCHO, and NO_3, were measured by the University of Houston using a Scanning Actinic Flux Spectroradiometer (SAFS) while the remaining photolysis frequencies were estimated and then scaled to either measured $J(NO_2)$ or $J(O_1D)$ values. The University of Wisconsin measured glyoxal using a laser induced phosphorescence (LIP) instrument. Nitrous acid was measured by the State University of New York-Albany using a wet chemical technique.

$$[OH] = \frac{S_{OH}}{C_{OH}} \qquad \text{(Equation 5)}$$

Table 1: Investigators and measurements

Measurement	Investigator	Method	Height
Prophet Tower			
Gas Phase HOx Chemistry			
OH/HO_2, OH reactivity	Stevens (Indiana)	LIF	top of tower, forest floor
Photolysis rates at top of tower	Lefer (Houston)	Spectral radiometer	top of tower
Horiontal & vertical UV distribution	Lefer (Houston)		through canopy
VOC flux and ambient concentrations	Jobson (WSU)	GC-MS, PTR-MS	top of tower, through canopy
Above-canopy BVOC flux	Guenther (NCAR)	REA/GCMS	top of tower
NO_x	Carroll (Michigan)	chemiluminescence	top of tower
O_3, CO	Carroll (Michigan)	TEI absorption	top of tower
Total organic nitrates, total PANs	Shepson (Purdue)	thermal conversion	top of tower
Glyoxal, formaldehyde	Keutsch (Wisconsin)	LIP/LIF	top of tower through canopy, fluxes
HONO profile	Zhou (Wadsworth)	Scrubbing derivatization	above & below top of tower
Modeling of 1D & canopy-scale chemistry	Steiner (Michigan) Guenther (NCAR)	CACHE model	through canopy
Enclosure Emissions & Oxidant Loss Frequency Assessment			
Soil VOC fluxes	Guenther (NCAR)	Enclosure & PTR-MS/GCMS	forest floor
Branch & soil OH reactivity	Guenther (NCAR)	Enclosure & PTR-MS	forest floor
BVOC emissions speciation & rates	Helmig (Colorado)	Leaf/branch enclosures/GCMS	forest floor & canopy
O_3 reactivity of BVOC emissions	Helmig (Colorado)	Leaf/branch enclosures/differential O_3 measurement	forest floor & canopy
Pine leaf VOC concentration	Bertman (Western Mich)	GCMS	forest floor
Particle Formation Chemistry			
Particle size distribution	VanReken (Wash St)	Multiple SMPS	3 heights through canopy

	Lee (Kent State)		
Water soluble particle composition	VanReken (Wash St)	PILS-IC-TOC	forest floor
gas-phase H_2SO_4 & NH_3	Lee (Kent State)	CIMS	top of tower
PBL height & aerosol distribution	Lamb (Wash St)	Aerosol Lidar	through BL
Aerosol scattering properties	VanReken (Wash St)	Nephelometers	2 heights in canopy
Particle-phase glyoxal, methyglyoxal and organosulfates	Keutsch (Wisconsin)	Filter sampler	Above canopy
FASET Tower			
BVOC fluxes	Guenther (NCAR)	REA/GCMS	top of tower
Photolysis rates at top of tower	Lefer (Houston)	Spectral radiometer	top of tower
Horizontal & vertical UV distribution	Lefer (Houston)		through canopy
BVOC emissions speciation & rates	Helmig (Colorado)	Leaf/branch enclosures,GCMS	forest floor & canopy
O_3 reactivity of BVOC emissions	Helmig (Colorado)	Differential O_3 measurement	forest floor & canopy
ALAR (Airborne Laboratory for Atmospheric Research)			
BVOC fluxes & vertical profiles	Shepson (Purdue)	DEA	up to 5 km
Analysis of BVOC in DEA samples	Guenther (NCAR)	GCMS/PTRMS	up to 5 km
Vertical profiles of aerosol	Shepson (Purdue)	SMPS	up to 5 km

Model

In order to validate data from the *in situ* measurements made during the 2009 CABINEX field campaign at UMBS the system was modeled using zero-dimensional or static box models which have been used successfully in the past, e.g ; Crawford et al. (1997), Carslaw et al. (1999), Zanis (1999), Klem et al. (2000), Carpenter et al. (2000). Two additional models were evaluated for the CABINEX and previous PROPHET field campaigns with varying success by other groups. Bryan et al. (2012) utilized a 1-D canopy model in an attempt to better understand ozone

precursors and secondary ozone production. They utilized the Canopy Atmospheric Chemistry Emission (CACHE) using the biogenic chemistry from the Regional Atmospheric Chemistry Model (RACM) in addition to the RACM with additional isoprene chemistry from the Mainz isoprene mechanism. The simplified model showed difficulties in capturing the HOx chemistries and BVOC oxidation products. The inclusion of advanced isoprene chemistries shows negligible improvement to the model. Griffith et al. (2013) again utilized RACM and the Mainz isoprene mechanism to generate a zero-dimensional box model. The results from this study showed generally good agreements between the observed and measured OH radical concentrations with a ratio of 0.70 ± 0.31. The authors mention that this agreement is generally not observed and may be a result of the lower than average temperature observed during the CABINEX campaign.

FACSIMILE is an ordinary differential equation solver written in a proprietary high level programming language used for numerical analysis and the modeling of chemical kinetics and transport (Curtis and Sweetenham, 1987). In this language, chemical reactions, ordinary differential equations, and boundary conditions can be expressed efficiently and neatly as seen in Equation *6*. Here F<008> represents the function number followed by the rate equation for the oxidation of H_2O via $O(^1D)$.

$$F < 008 > \ \% \ 1.63D - 10 * EXP(60/TEMP) \qquad : \ OD + H_2O \ = \ OH + OH \ ;$$

Equation 6: Oxidation of H_2O via $O(^1D)$

The relationship between the production of ozone and varying VOC and peroxy radical concentrations was modeled utilizing a photochemical box model based on the work done by Zanis (1999) and Edwards (2000). The model described here included the photolysis of O_3, NO_2, N_2O_5, H_2O_2, HONO, HNO_3, HCHO, CH_3O_2H, HO_2NO_2, CH_3CHO, C_3H_7CHO, C_2H_5CHO, and

CH_3COCH_3. Table 2 shows the complete chemical scheme. Use of such a simple chemical scheme can be justified by the observed data from the 2009 CABINEX field campaign.

Table 2: Reaction pathways and kinetic coefficients utilized in the photochemical box model. Temp is the absolute temperature (K), M is the concentration of air molecules (molecules cm^{-3}) and J is the photolysis rate constant (s^{-1}).

Reaction number	Rate Equation	Equation
F<000>	6.0D-34*M*(TEMP/300.)@-2.3	$O+O_2 = O_3$
F<001>	5.1D-12*EXP(210.0/TEMP)	$O+NO_2 = NO$
F<002>	9.0D-31*M*(TEMP/300.)@-2.0	$O+NO_2 = NO_3$
F<003>	2.2D-11*EXP(120./TEMP)	O+OH = H
F<004>	3.0D-11*EXP(200./TEMP)	$O+HO_2 = OH$
F<005>	9.0D-32*M*(TEMP/300.)@-1.5	$O+NO = NO_2$
F<006>	8.0D-12*EXP(-2060./TEMP)	$O+O_3 = O_2$
F<007>	2.1D-11*M*EXP(100.0/TEMP)	OD = O
F<008>	1.63D-10*EXP(60/TEMP)	$OD+H_2O = OH+OH$
F<009>	4.4D-32*M*(TEMP/300.0)@-1.3	$H+O_2 = HO_2$
F<010>	J<0>	$O_3 = O$
F<011>	J<1>	$O_3 = OD$
F<012>	3.0D-12*EXP(-1500./TEMP)	$O_3+NO = NO_2$
F<013>	1.2D-13*EXP(-2450./TEMP)	$O_3+NO_2 = NO_3$
F<014>	1.7D-12*EXP(-940./TEMP)	$O_3+OH = HO_2$
F<015>	1.1D-14*EXP(-490./TEMP)	$O_3+HO_2 = OH$
F<016>	1.5D-11*EXP(170./TEMP)	$NO+NO_3 = NO_2+NO_2$
F<017>	7.0D-31*M*(TEMP/300.)@-2.6	NO+OH = HONO
F<018>	8.2D-39*H2O	$NO+NO_2$ = HONO+HONO
F<019>	1.6D-24	HONO+HONO = $NO+NO_2$
F<020>	3.5D-12*EXP(250./TEMP)	$NO+HO_2 = NO_2+OH$
F<021>	J<4>	$NO_2 = NO+O$
F<022>	4.5D-14*EXP(1260./TEMP)	$NO_2+NO_3 = NO+NO_2$
F<023>	2.0D-30*M*(TEMP/300.)@-4.4	$NO_2+NO_3 = N_2O_5$
F<024>	1.8D-30*M*(TEMP/300.)@-3.2	$NO_2+OH = HNO_3$
F<025>	1.8D-31*M*(TEMP/300.)@-3.2	$NO_2+HO_2 = HO_2NO_2$
F<026>	5.0D-6*M*EXP(-10000./TEMP)	$HO_2NO_2 = NO_2+HO_2$
F<027>	J<9>	$NO_3 = NO$
F<028>	J<13>	$NO_3 = NO_2+O$
F<029>	4.1D-16	$NO_3+H_2O_2 = HO_2+HNO_3$
F<030>	8.5D-13*EXP(-2450./TEMP)	$NO_3+NO_3 = NO_2+NO_2$
F<031>	J<5>	$N_2O_5 = NO_2+NO_3$
F<032>	1.7D+17*EXP(-12450./TEMP)	$N_2O_5 = NO_2+NO_3$

F<033>	2.0D-21	$N_2O_5+H_2O = HNO_3+HNO_3$
F<034>	4.8D-11*EXP(250./TEMP)	$OH+HO_2 = H_2O + O_2$
F<035>	2.9D-12*EXP(-160./TEMP)	$OH+H_2O_2 = HO_2$
F<036>	J<2>	$H_2O_2 = OH+OH$
F<037>	2.8D-12*EXP(-1800./TEMP)	$OH+H_2 = H$
F<038>	1.8D-11*EXP(-390./TEMP)	$OH+HONO = NO_2$
F<039>	9.4D-15*EXP(778./TEMP)	$OH+HNO_3 = NO_3$
F<040>	(2.3D-13*EXP(600./TEMP)+1.7D-33*N2*EXP(1000./TEMP))*(1+1.4E-21*H2O*EXP(2200./TEMP))	$HO_2+HO_2 = H_2O_2$
F<043>	J<8>	$HONO = NO+OH$
F<044>	J<3>	$HNO_3 = NO_2+OH$
F<045>	1.35D-12	$OH+SO_2 = HSO_3$
F<046>	4.0D-17	$CH_3O_2+SO_2 = SO_3+CH_3O$
F<047>	4.0D-32*M*EXP(-1000./TEMP)	$O+SO_2 = SO_3$
F<048>	1.0D-18	$HO_2+SO_2 = SO_3+OH$
F<049>	1.0D-11	$HSO_3+O_2 = HO_2+SO_3$
F<050>	9.1D-13	$SO_3+H_2O = SA$
F<067>	2.45D-12*EXP(-1775./TEMP)	$OH+CH_4 = CH_3$
F<068>	4.0D-31*M*(TEMP/300.)@-3.6	$CH_3+O_2 = CH_3O_2$
F<069>	2.8D-12*EXP(300./TEMP)	$CH_3O_2+NO = CH_3O+NO_2$
F<070>	9.5D-14*EXP(390./TEMP)	$CH_3O_2+CH_3O_2 = CH_3O+CH_3O$
F<071>	6.8D-14*EXP(220./TEMP)	$CH_3O_2+CH_3O_2 = CH_3OH+HCHO$
F<072>	2.9D-12*EXP(-345./TEMP)	$CH_3OH+OH = HO_2+HCHO$
F<073>	7.0D-12*EXP(-235./TEMP)	$C_2H_5OH+OH=CH_3CHO+HO_2$
F<074>	3.8D-13*EXP(800./TEMP)	$HO_2+CH_3O_2 = CH_3O_2H$
F<075>	3.9D-14*EXP(-900./TEMP)	$CH_3O+O_2 = HCHO+HO_2$
F<076>	1.1D-11	$OH+HCHO = HO_2+CO$
F<077>	J<6>	$HCHO = H+CO+HO_2$
F<078>	J<7>	$HCHO = H_2+CO$
F<079>	5.8D-16	$NO_3+HCHO = HNO_3+CO+HO_2$
F<080>	2.4D-13	$OH+CO = CO_2+H$
F<081>	J<11>	$CH_3O_2H=CH_3O+OH$
F<082>	J<12>	$HO_2NO_2=HO_2+NO_2$
F<181>	8.7D-12*EXP(-1070./TEMP)	$OH+C_2H_6 = C_2H_5O_2$
F<182>	2.6D-12*EXP(365./TEMP)	$C_2H_5O_2+NO = C_2H_5O+NO_2$
F<083>	2.5D-14	$C_2H_5O_2+CH_3O_2 = CH_3O+C_2H_5O$
F<084>	33	$C_2H_5O = HCHO+CH3$
F<085>	6.3D-14*EXP(-550./TEMP)	$C_2H_5O+O_2 = HO_2+CH_3CHO$
F<086>	J<10>	$CH_3CHO = CH_3+HO_2+CO$
F<087>	6.0D-12*EXP(250./TEMP)	$OH+CH_3CHO = CH_3COO_2$
F<088>	1.4D-12*EXP(-1900./TEMP)	$NO_3+CH_3CHO = HNO_3+CH_3COO_2$

F<089>	8.0D-29*M*(TEMP/300.)@-7.0	$CH_3COO_2+NO_2$ = PAN
F<090>	3.2D-5*EXP(-12500./TEMP)	PAN = $CH_3COO_2+NO_2$
F<091>	2.4D-11	$CH3COO_2+NO = NO_2+CH_3+CO_2$
F<092>	1.4D-11	$CH_3O_2+CH_3COO_2=CH_3O+CH_3+CO_2$
F<093>	6.7D-13	$C_2H_5COO_2+NO=NO_2+C_2H_5O_2+CO_2$
F<094>	2.5D-14	$C_2H_5COO_2+CH_3O_2=CH_3O+C_2H_5O_2$
F<095>	3.9D-13	$C_2H_5COO_2+NO_2$=PPN
F<096>	7.94D+14*EXP(-12530./TEMP)	PPN=$C_2H_5COO_2+NO_2$
F<100>	1.9D-11	$C_3H_7CHO+OH = C_3H_7COO_2$
F<101>	3.7D-13	$NC_3H_7O_2+NO=NC_3H_7O+NO_2$
F<102>	2.5D-14	$CH_3O_2+NC_3H_7O_2=CH_3O+NC_3H_7O$
F<103>	3.7D-17*O2	$NC_3H_7O=C_2H_5CHO+HO_2$
F<106>	1.9D-11	$C_2H_5CHO+OH = C_2H_5COO_2$
F<107>	1.6D-11*EXP(-800./TEMP)	$C_3H_8+OH = NC_3H_7O_2$
F<108>	1.66D-12*EXP(474./TEMP)	$C_2H_4+OH = CH_2O_2CH_2OH$
F<109>	3.1D-13	$CH_2O_2CH_2OH+NO=CH_2OCH_2OH+NO_2$
F<110>	2.5D-14	$CH_3O_2+CH_2O_2CH_2OH=CH_3O+CH_2OCH_2OH$
F<111>	4.3D-16*O2	$CH_2OCH_2OH=HO_2+HCHO+HCHO$
F<112>	1.2D-14*EXP(-2633./TEMP)	$C_2H_4+O_3 = HCHO+CH_2OO$
F<113>	4.3D-16*O2	CH_2OO=,*0.12:HO_2,*0.12:H_2
F<114>	1.6D-11*EXP(-800/TEMP)	$C_3H_8+OH = SECC_3H_7O_2$
F<123>	3.1D-13	$NO+CH_3COCH_2O_2=NO_2+CH_3COCH_2O$
F<124>	2.5D-14	$CH_3O_2+CH_3COCH_2O_2=CH_3O+CH_3COCH_2O$
F<125>	3.7D-17*O2	CH_3COCH_2O=MGLYOX+HO_2
F<126>	6.5D-15*EXP(-2105./TEMP)	$O_3+C_3H_6$ = HCHO,*0.29:HO_2=,*0.19:OH,*0.05:CH_3O,*0.43:CH_3O_2
F<127>	6.5D-15*EXP(-2105./TEMP)	$O_3+C_3H_6 = CH_3CHO$,*0.12:HO_2,*0.12:H_2
F<128>	4.1D-12*EXP(545./TEMP)	$OH+C_3H_6 = CH_3CHO_2CH_2OH$
F<131>	4.3D-16*O2	$CH_3CHOCH_2OH=CH_3CHO+HCHO+HO_2$
F<132>	1.6D-12	$CH_3O_2 + NO_2 = MEO_2NO_2$
F<133>	1.2D+15*EXP(-10580/TEMP)	$MEO_2NO_2 = CH_3O_2+NO_2$
F<137>	2.54D-11*EXP(410/TEMP)*0.66	$OH+C_5H_8 = IPR_{12}$
F<138>	2.54D-11*EXP(410/TEMP)*0.34	$OH+C_5H_8 = IPR_{45}$
F<139>	2.54D-12*EXP(360/TEMP)*0.892	IPR_{12}+NO = MVK + HCHO
F<140>	2.54D-12*EXP(360/TEMP)*0.892	IPR_{45}+NO = MCAR + HCHO
F<141>	7.86D-15*EXP(-1913/TEMP)*0.2	$O_3 + C_5H_8$ = CH_2OOE + MVK
F<142>	7.86D-15*EXP(-1913/TEMP)*0.2	$O_3 + C_5H_8$ = HCHO + MVKOOA
F<143>	7.86D-15*EXP(-	$O_3 + C_5H_8 = CH_2OOE$ + MCAR

	1913/TEMP)*0.3	
F<144>	7.86D-15*EXP(-1913/TEMP)*0.3	$O_3 + C_5H_8 = HCHO + MACROOA$
F<145>	1.20D-11*EXP(444/TEMP)*0.572	$APINE + OH = APINAO_2$
F<146>	1.20D-11*EXP(444/TEMP)*0.353	$APINE + OH = APINBO_2$
F<147>	1.20D-11*EXP(444/TEMP)*0.075	$APINE + OH = APINCO_2$
F<148>	2.54D-12*EXP(360/TEMP)*0.770	$APINAO_2 + NO = APINAO + NO_2$
F<149>	2.54D-12*EXP(360/TEMP)*0.230	$APINAO_2 + NO = APINANO_3$
F<150>	2.54D-12*EXP(360/TEMP)*0.770	$APINBO_2 + NO = APINBO + NO_2$
F<151>	2.54D-12*EXP(360/TEMP)*0.230	$APINBO_2 + NO = APINBNO_3$
F<152>	2.54D-12*EXP(360/TEMP)*0.875	$APINCO_2 + NO = APINCO + NO_2$
F<153>	2.54D-12*EXP(360/TEMP)*0.125	$APINCO_2 + NO = APINCNO_3$
F<154>	2.38D-11*EXP(357/TEMP)*0.849	$BPINENE + OH = BPINAO_2$
F<155>	2.38D-11*EXP(357/TEMP)*0.076	$BPINENE + OH = BPINBO_2$
F<156>	2.38D-11*EXP(357/TEMP)*0.075	$BPINENE + OH = BPINCO_2$
F<157>	1.50D-17*0.6	$BPINENE + O_3 = NOPINOOA + HCHO$
F<158>	1.50D-17*0.4	$BPINENE + O_3 = NOPINONE + CH_2OOF$
F<159>	2.38D-11*EXP(357/TEMP)*0.760	$BPINAO_2 + NO = BPINAO + NO_2$
F<160>	2.38D-11*EXP(357/TEMP)*0.240	$BPINAO_2 + NO = BPINANO_3$

The photolysis rate constants $j(O^1D)$ and $j(NO_2)$ were measured *in situ* from the AmeriFlux tower. The cross sections and quantum yields for the different species were taken from the recommended data of Atkinson et al. (2004, 2006). The calculated photolysis frequencies were corrected for cloud and aerosol effects by scaling to the measured $j(NO_2)$. In general, photolysis rates are parameterized as a function of solar zenith angle, X, as seen in

(*Equation* 7. In each case, variation of photolysis rates with solar zenith angle can be described well by optimizing the values of the three parameters, l, m and n in (Equation 7) (Jenkin et al., 1997).

$$J = l * cosX@m * EXP(-n * secX) \quad \text{(Equation 7)}$$

***In Situ* Photolysis Calculation**

Variations in actinic flux from day to day during the campaign (e.g. resulting from cloud cover) can be accounted for by considering the difference between measured and calculated $j(NO_2)$ at any given time during the experiments. Values for other photolysis frequencies not measured but still required to constrain the model were estimated from the Tropospheric Ultraviolet-Visible (TUV 4.1) model (Madronich 1987), and then scaled to the calculated fit of $j(NO_2)$ derived from the actinic flux measurements as described below. J<4> is the measured photolysis frequency for NO_2, using the theoretical photolysis values from (Equation 7; the ratio $j_{unknown}/j(NO_2)$ can be used to calculate the necessary photolysis values.

$$\mathrm{J<4>} = \text{measured j}(NO_2); \quad \text{(Equation 8)}$$

$$\mathrm{J<1>} = 0.3612 * \mathrm{J<4>@02} - 0.0004 * \mathrm{J<4>}; \quad \text{(Equation 9)}$$

$$\mathrm{J<3>} = 0.006 * \mathrm{J<4>@02 + 1D - 05 * J<4>}; \quad \text{(Equation 10)}$$

Figure 4 and Figure 5 show hour-averaged peroxy radical concentrations versus $j(O^1D)$ and the square root of the photolysis frequency, SQRT($j(O^1D)$) respectively from 6:00 to 21:00. It was shown during the Southern Ocean Atmospheric Photochemistry Experiment in the Southern Ocean at Cape Grim, Tasmania that in unpolluted marine air, the sum of the peroxy

radicals HO_2 + RO_2 is proportional to the square root of $j(O^1D)$, and in semi-polluted air is proportional to the first order of $j(O^1D)$ (Penkett et al., 1997). Due to the small sampling of $j(O^1D)$ measurements a full day's worth of measurements were used for this analysis. If a larger data set was available, only measurement from the morning to mid-day would be used, as the measurements observed in the afternoon generally show a different trend (Monks, Carpenter, Penkett, & Ayers, 1996). Visual inspection of the plots alone does not yield much information about the dependence of the concentration of OH and HO2 on $j(O^1D)$ or SQRT($j(O^1D)$).

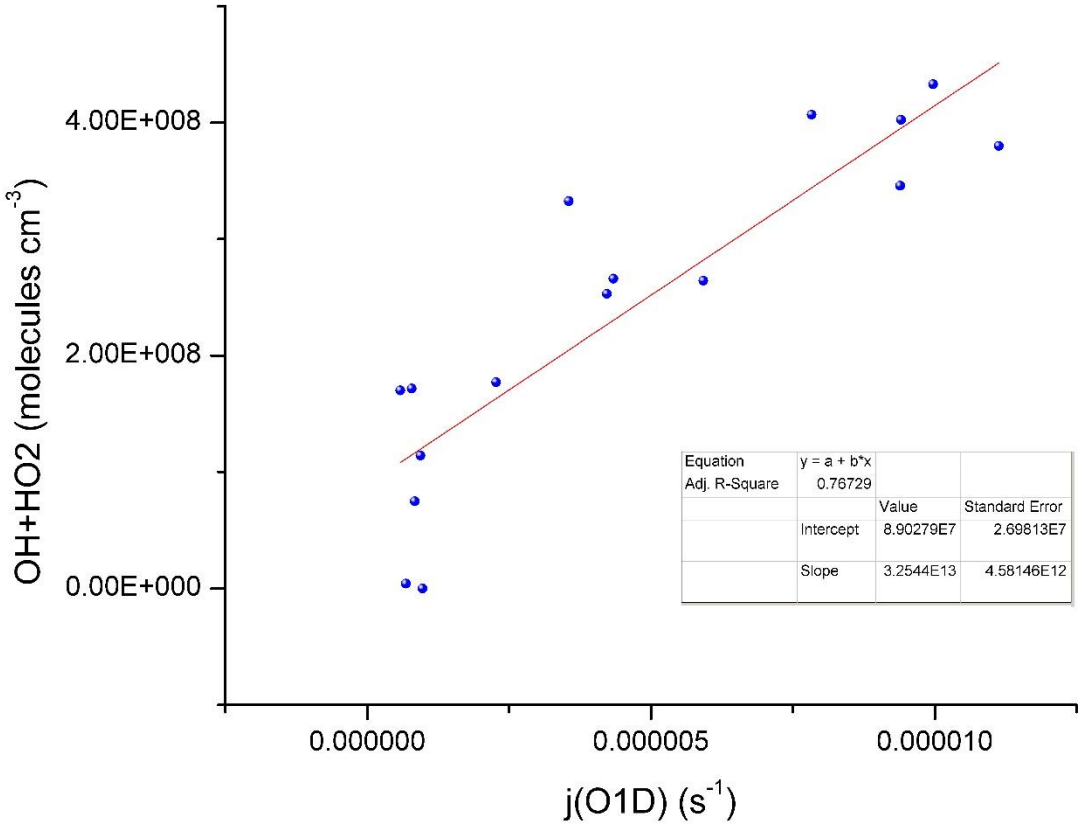

Figure 4: Scatter plot of hour averaged peroxy radical concentrations versus $j(O^1D)$ from 6:00 am to 21:00 pm.

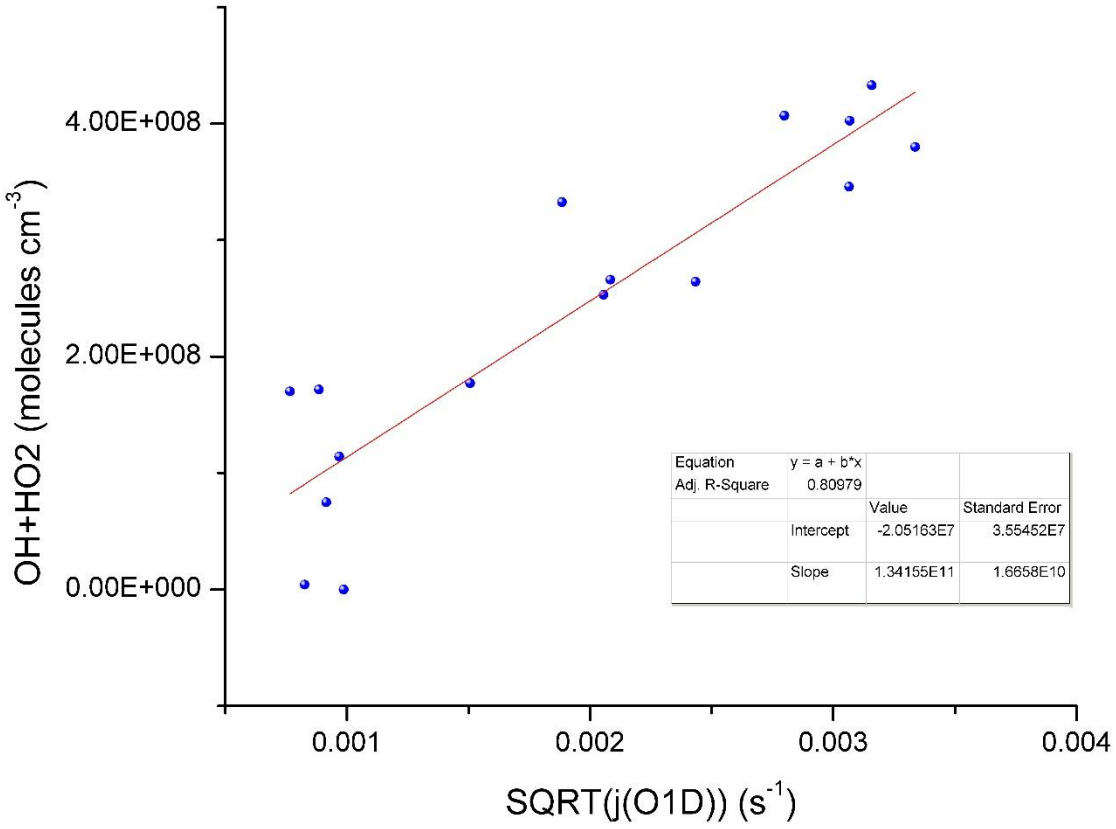

Figure 5: Scatter plot of hour averaged peroxy radical concentrations versus SQRT(j(O^1D)) from 6:00 am to 21:00 pm.

The residual sum of squares was calculated from the fitted regression lines of Figure 4 and Figure 5. An ANOVA F-test was used to compare the data in Figure 4 and Figure 5 in order to determine which calculated regression line best fits the data. The ANOVA F-test is useful when comparing statistical models that have been fitted to a data set in order to identify the model that best fits the population from which the data were sampled (Bernhardson, C., 1975). The F-ratio, computed in Origin Pro, is 47.54, which is greater than the critical value at the 95% significance level of 3.34. A null hypothesis was made stating there is no improvement in in the model OH + HO_2 vs. $j(O^1D)$ when the proposed alternative model, OH + HO_2 vs SQRT($j(O^1D)$) is used. The

critical value is the number that the test statistic must exceed to reject the null hypothesis. This indicates that the null model is to be rejected. The better dependence of peroxy radical concentrations on the SQRT($j(O^1D)$) indicates a relatively clean atmosphere. To further confirm this, the ratio of hydroperoxy to the hydroxide radical was investigated. The average ratio was found to be 132.24 which has also been shown to be indicative of a clear air environment (Creasey et al., 2003; Hofzumahaus et al., 2009; Monks et al., 1996).

Figure 6 shows the average ozone concentration for the CABINEX campaign along with the observed concentrations for days in which HO_x measurements were made. Observed during this campaign was a lack of ozone destruction, which would be expected in a clean environment with HO_x showing a good square root dependence on $j(O^1D)$. It is worth noting that of the days in which HO_x measurements were made, ozone data recorded on the 8th are statistically different than the average. On July 25th and August 8th there were noteworthy spikes in the ozone concentration. It cannot be assumed that ozone changes observed during this campaign at UMBS are solely influenced by photochemistry.

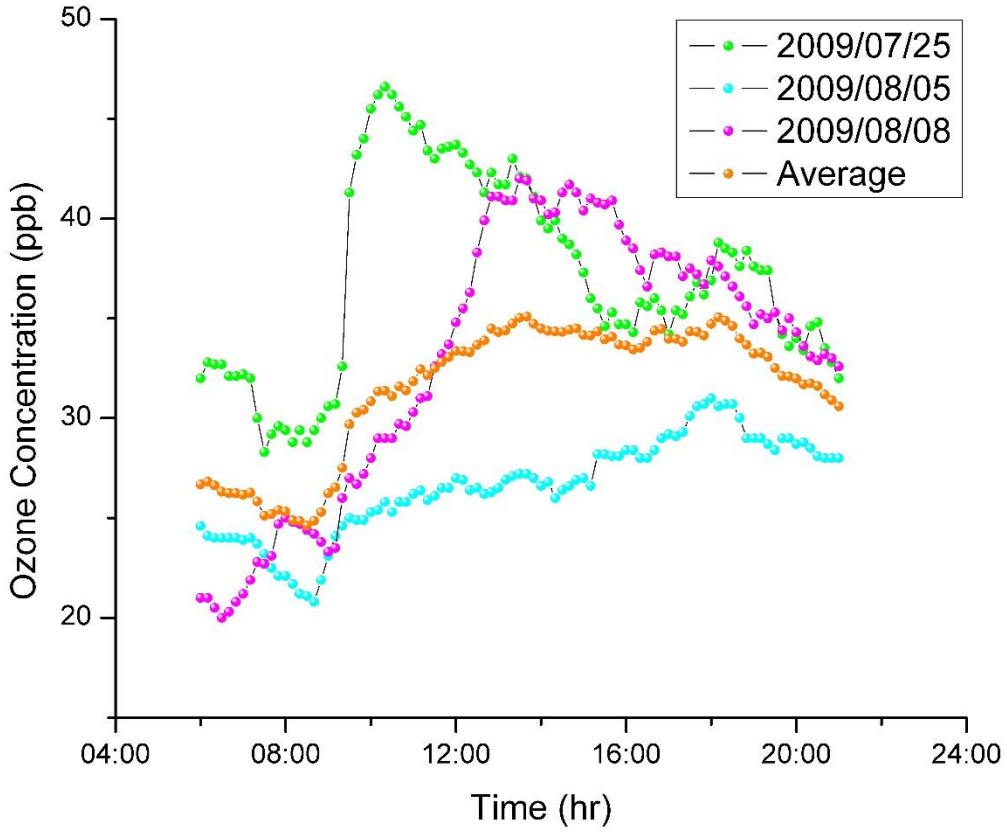

Figure 6: Half-hourly average ozone cycle for days in which HO_x measurements were made as well.

Recent literature contains several examples comparing modeled to measured HO_x concentrations. In very clean environments there is often a disagreement between the modeled and measured concentration of HO_x in the form of an underestimation in the HO_x concentrations by the model (e.g. Bloss et al.,2010; Da Silva et al., 2010). This suggests that unmeasured HO_x precursors are not taken into account. An example could be the heterogeneous reaction of NO_2 with aerosols to form NO_3 and HONO after which HONO photolysis takes place, producing additional OH radicals. This underestimation can be seen in Figure 7a-c and Figure 8a-c. Instances where the value is zero are a result of instrument error.

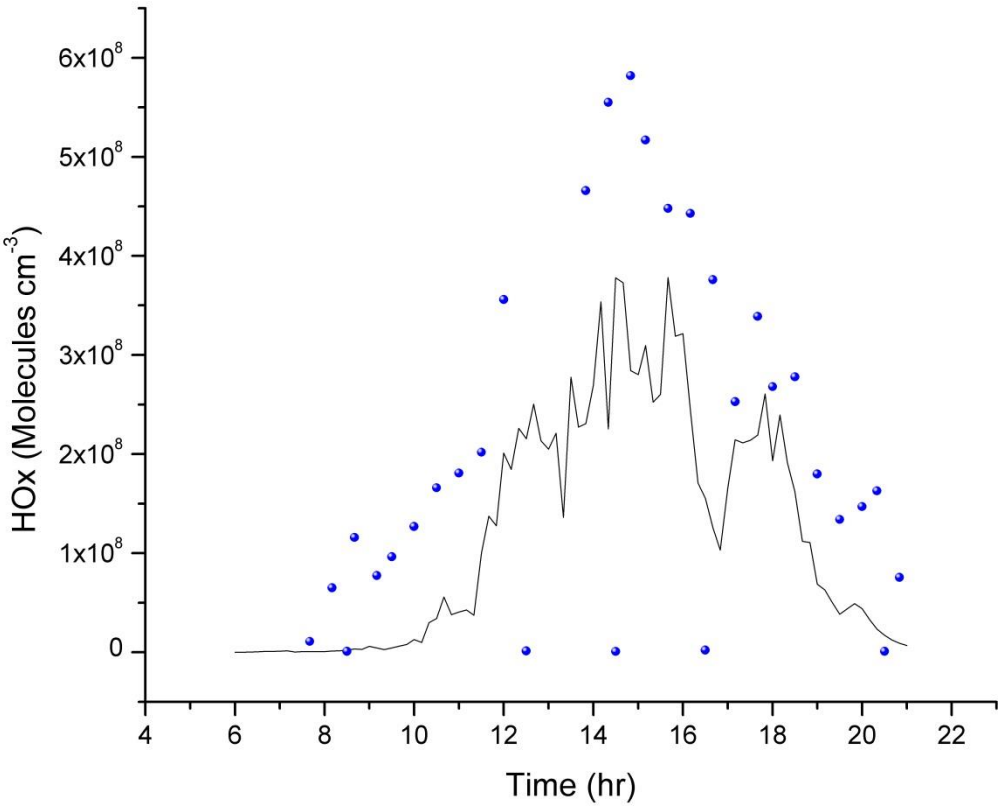
HOx (Molecules cm^{-3})
6x10^8
5x10^8
4x10^8
3x10^8
2x10^8
1x10^8
0
4
6
8
10
12
14
16
18
20
22
Time (hr)

a)

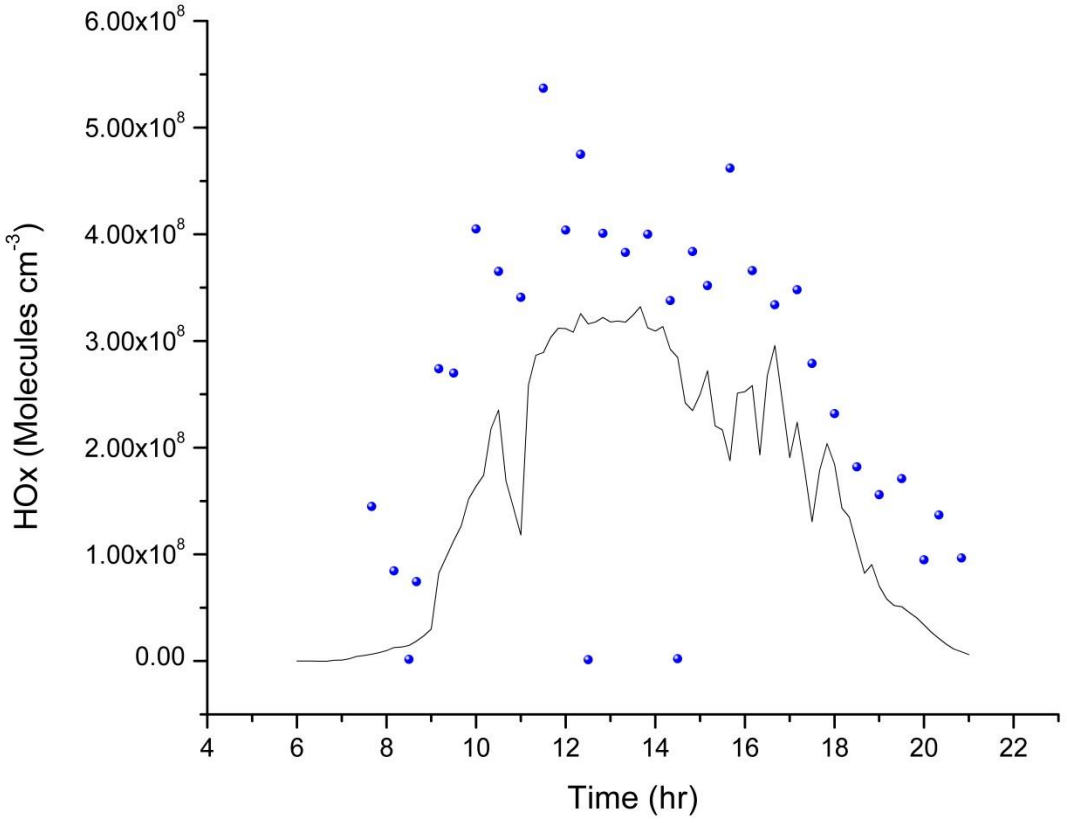
6.00x10^8
5.00x10^8
4.00x10^8
3.00x10^8
2.00x10^8
1.00x10^8
0.00
HOx (Molecules cm^-3)
4
6
8
10
12
14
16
18
20
22
Time (hr)

b)

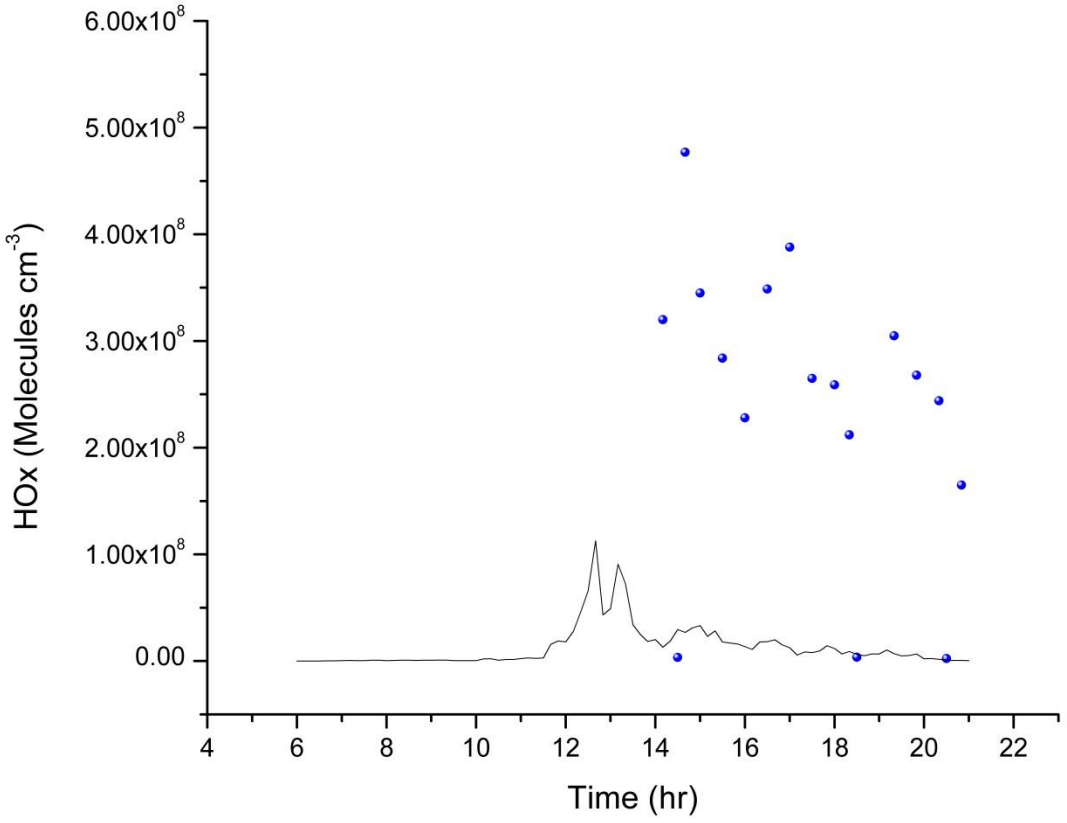

c)

Figure 7: Observed HO_x concentrations during the CABINEX campaign (blue spheres) in addition to modeled results (black line) for a) July 25, 2009 b) August 05, 2009 and c) August 08, 2009.

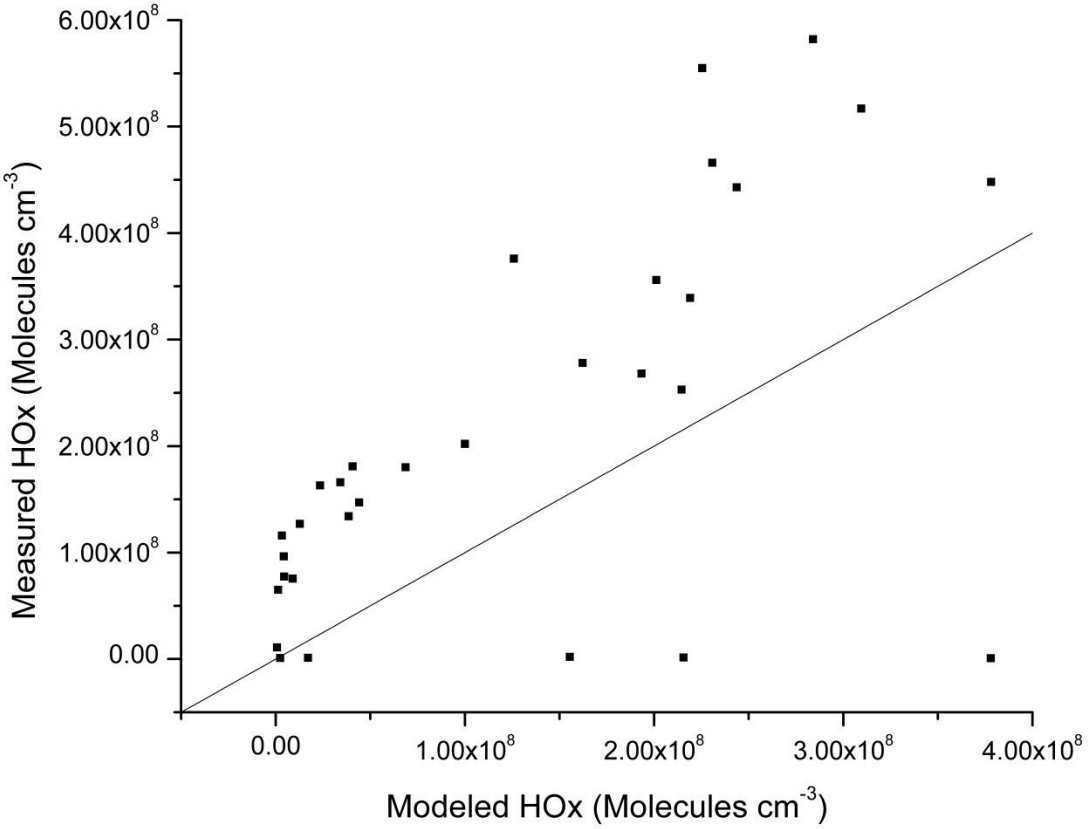
6.00x10^8
5.00x10^8
4.00x10^8
3.00x10^8
2.00x10^8
1.00x10^8
0.00
Measured HOx (Molecules cm^-3)
0.00
1.00x10^8
2.00x10^8
3.00x10^8
4.00x10^8
Modeled HOx (Molecules cm^-3)

a)

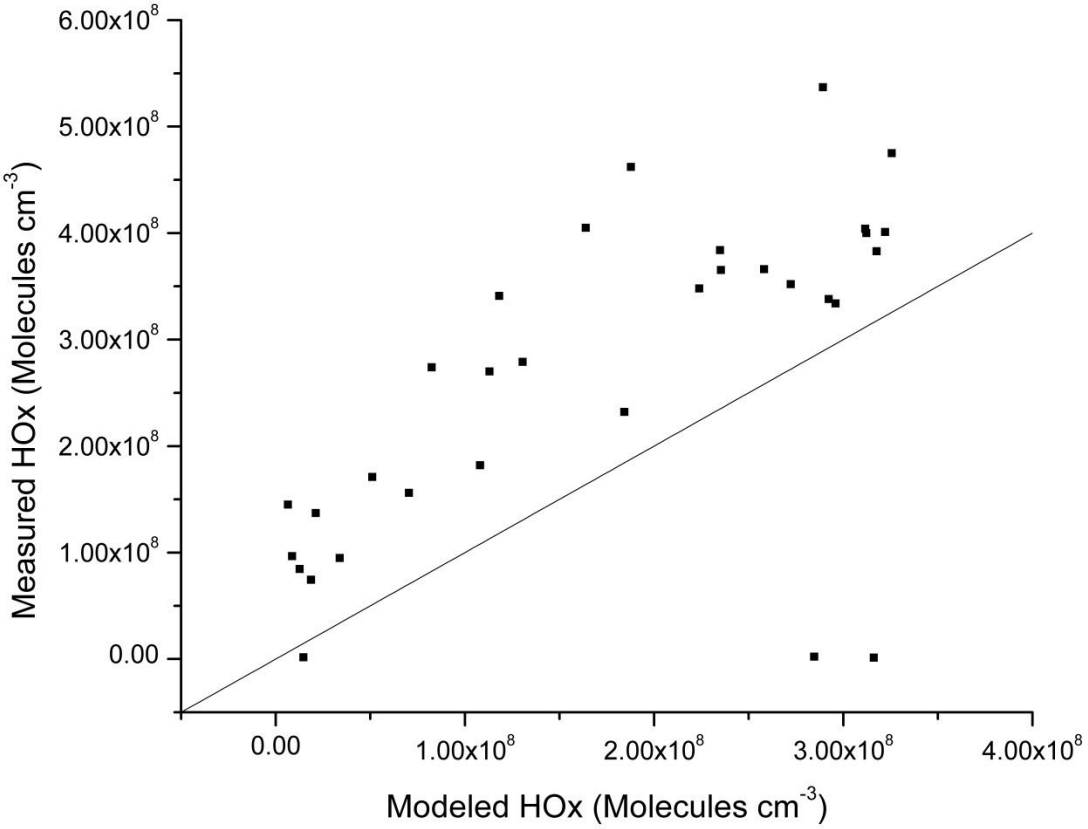
6.00x10^8
5.00x10^8
4.00x10^8
3.00x10^8
2.00x10^8
1.00x10^8
0.00
Measured HOx (Molecules cm^-3)
0.00
1.00x10^8
2.00x10^8
3.00x10^8
4.00x10^8
Modeled HOx (Molecules cm^-3)

b)

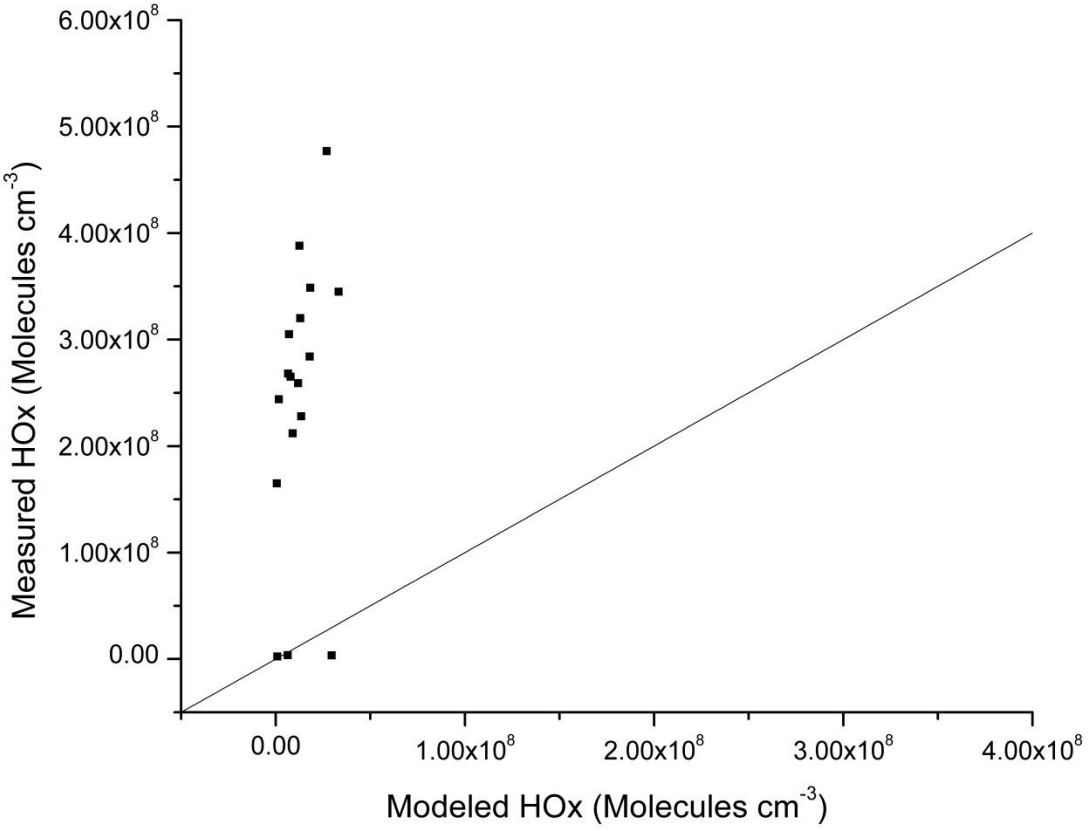

c)

Figure 8: Comparison of measured and modeled HO_x concentrations. The solid line represents the perfect match of simulation and observations. a) July 25, 2009 b) August 05, 2009 and c) August 08, 2009

In contrast, at "polluted" sites (Ren et al., 2006; Dusanter et al., 2009b) or in tropical forests (Kubistin et al., 2010; Stone et al., 2010), the models often overestimate the measured OH radical. This can be seen in Figure 9c, where the meteorological data suggest a potentially polluted air mass at the observational sight. In forests, this is possibly linked to the chemistry of secondary organic products from biogenic oxidation, or a source of radicals coming from

polluted environments the model does not account for (Butler et al., 2008; Lelieveld et al., 2008, Dusanter, 2009b).

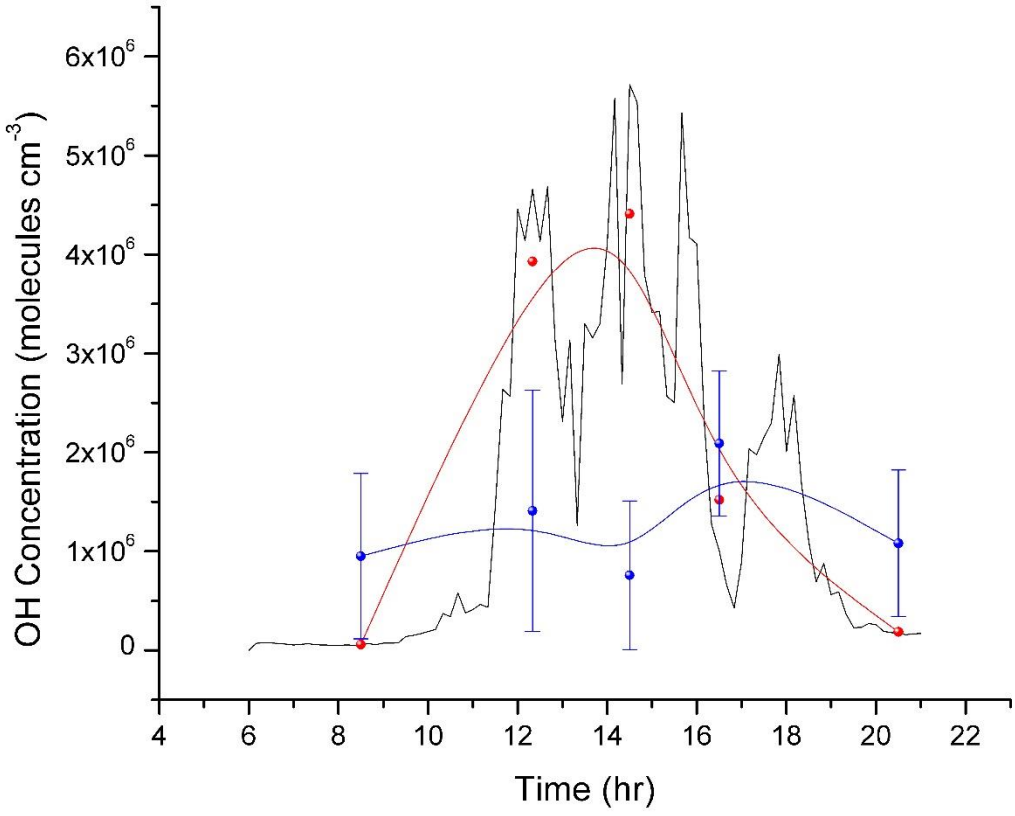

a)

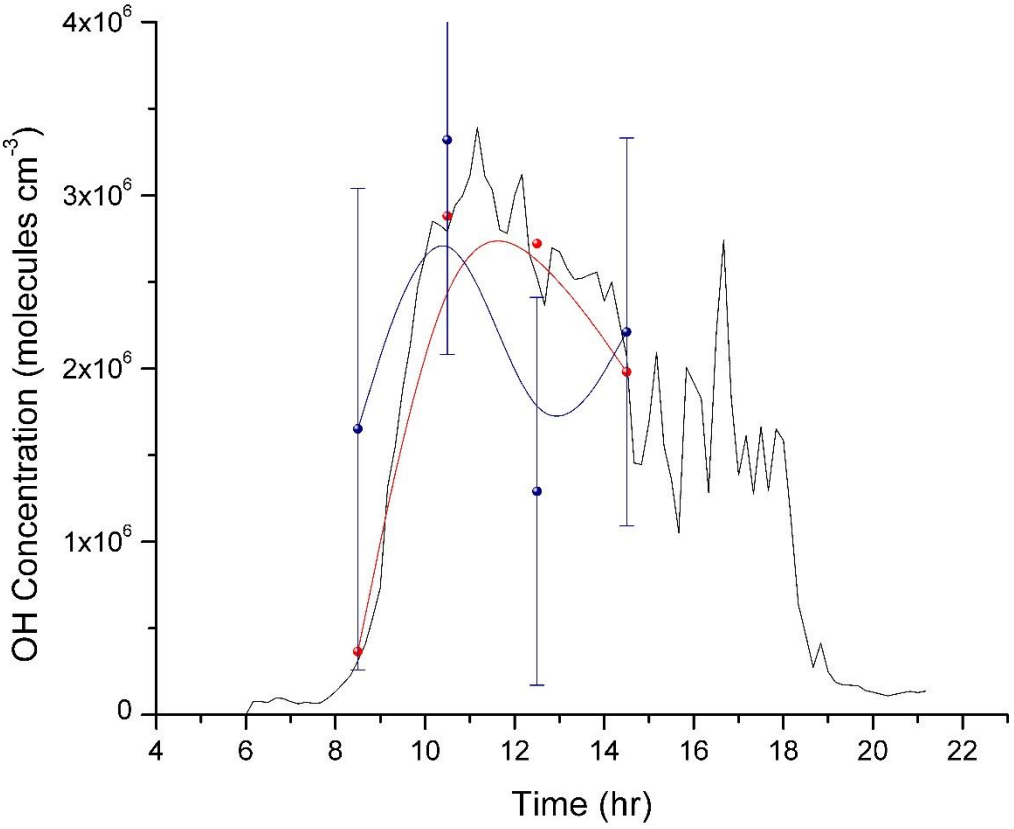
4x10^6
3x10^6
2x10^6
1x10^6
0
OH Concentration (molecules cm^-3)
4
6
8
10
12
14
16
18
20
22
Time (hr)

b)

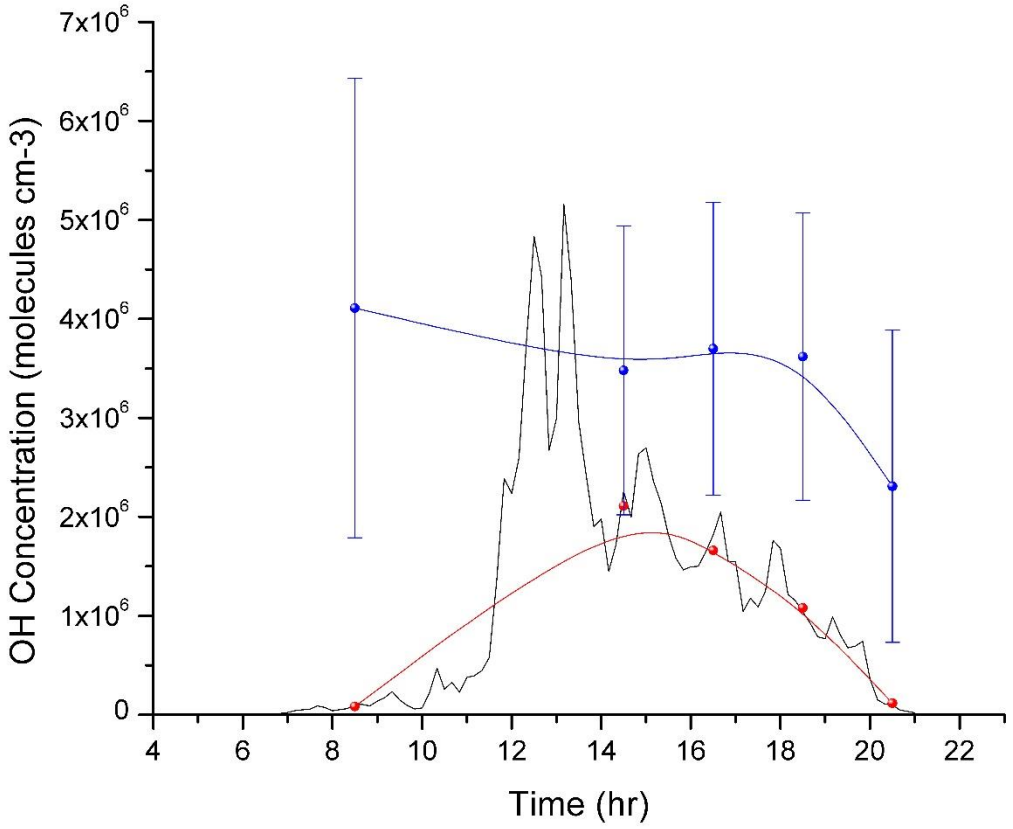

c)

Figure 9: Measured hydroxyl concentrations (blue spheres), where error bars are the precision (1 σ) compared to the modeled concentrations (red spheres) for a) July 25, 2009 b) August 05, 2009 c) August 08, 2009. The black line is the model output. Data were fitted with β-Spline function.

Summary

The model reproduced the qualitative behavior of HO_x but underestimated the observed levels. The underestimation of HO_x is similar to that seen using the MECCA model during the GABRIEL airborne field campaign over Suriname, French Guiana and Guyana (Kubistin et al., 2010). This underestimation of HO_x suggests there is a gap in the current understanding of the

influence of hydrocarbon emissions (specifically those of isoprene), or heterogeneous reactions with aerosols on HO_x chemistry. Butler et al. (2008) suggested that this underestimation may be a result of an incomplete understanding in the isoprene oxidation mechanism. They introduced an additional recycling mechanism (equivalent to (Equation 11) which better reproduced the observed HO_x concentrations. They did not speculate as to a source for the missing OH radical only as to its magnitude.

$$C_5H_8 + OH \rightarrow ISO_2 + OH \qquad \textit{(Equation 11)}$$

Atmospheric Transport

A sudden rise in NO_x concentrations on July 25 and August 08 during the CABINEX campaign suggests that the air masses over UMBS were not as clean as other days in which measurements were taken (Figure 10). Plotted with ozone and NO_x is PAR illustrating the influence of solar radiation on the diurnal profile of ozone. PAR also gives a good indication as to the present cloud cover at the site while measurements were conducted. As described at the beginning of this work, if there is cloud cover present the radiative balance will be altered, affecting the temperature, humidity, and VOC emission levels.

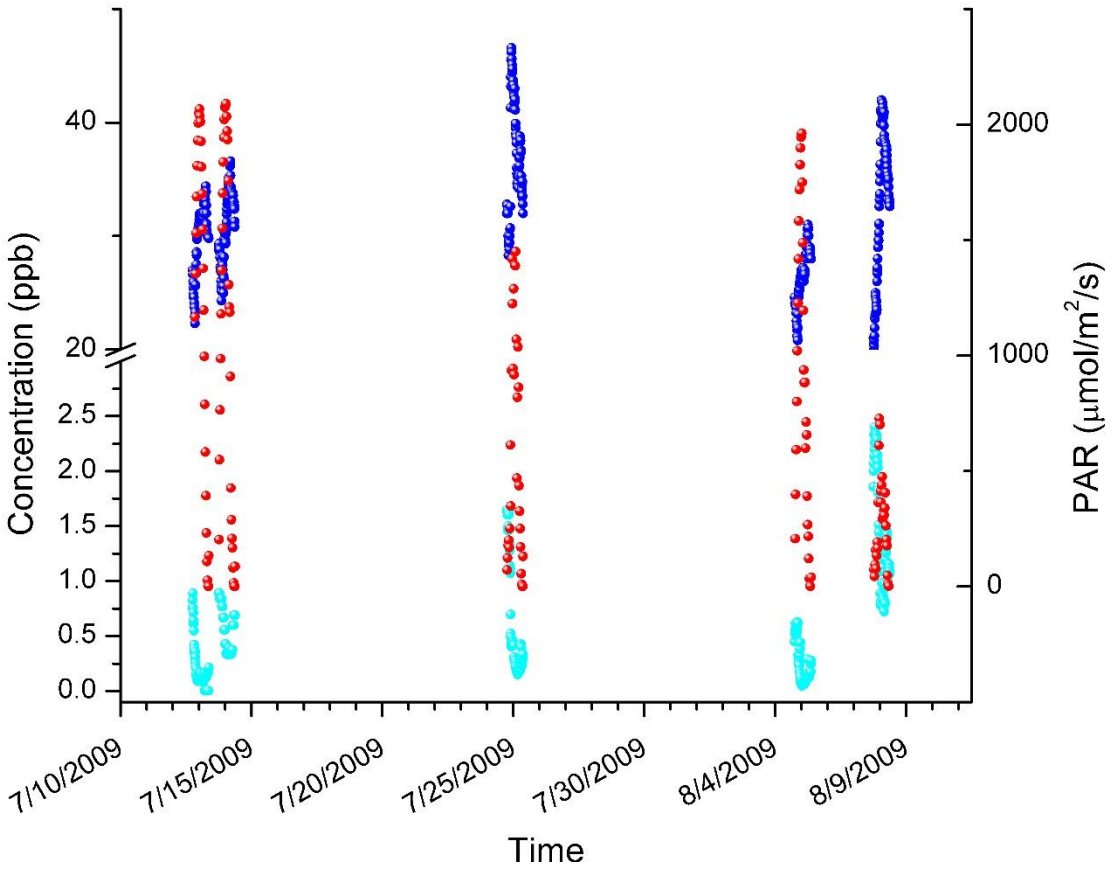

Figure 10: Plot of photosynthetically active radiation (PAR) red spheres, ozone (blue spheres), and NO_x (cyan spheres) for measurement days, with little to no cloud cover and little to no wind, during the CABINEX campaign.

This presence of elevated NO_x levels can be partially explained utilizing the Hybrid Single Particle Lagrangian Integrated Trajectory (HYSPLIT) model developed at the NOAA Air Resource Laboratory (Draxler and Rolph, 2013; Rolph, G. 2013). The HYSPLIT air trajectory model is capable of establishing source-receptor relationships over long distances. In order to extract information on the origin of the air masses, meteorological data from Global Data Assimilation System model outputs was used. 3-day back trajectories were selected because it is

sufficient to determine probable locations of regional emission sources and explain regional transport pathways without unnecessarily increasing uncertainty. July 25th seen in Figure 11a shows a North Westerly wind, then days prior to July 25th the winds moved over central and northern Wisconsin potentially transporting contaminated air from urban environments. Similar trends can be seen on August 8th and the days prior as seen in Figure 11c, where the air masses were not transported a significant distance on the 7th and remained over central Michigan and on August 8th. Southerly winds again could potentially transport air masses into the observational site contaminated with urban pollution. August 5th showed a lower NO_x concentration, and looking at the meteorological data on the days leading to the 5th it can be seen that there was a Westerly wind on the 4th followed by Northerly winds on the 5th. This would provide predominantly clean air to the observational site, see Figure 11b. The observed variation in NO_x concentrations indicates that the air above UMBS is not always well mixed and shows some dependency on wind direction and strength.

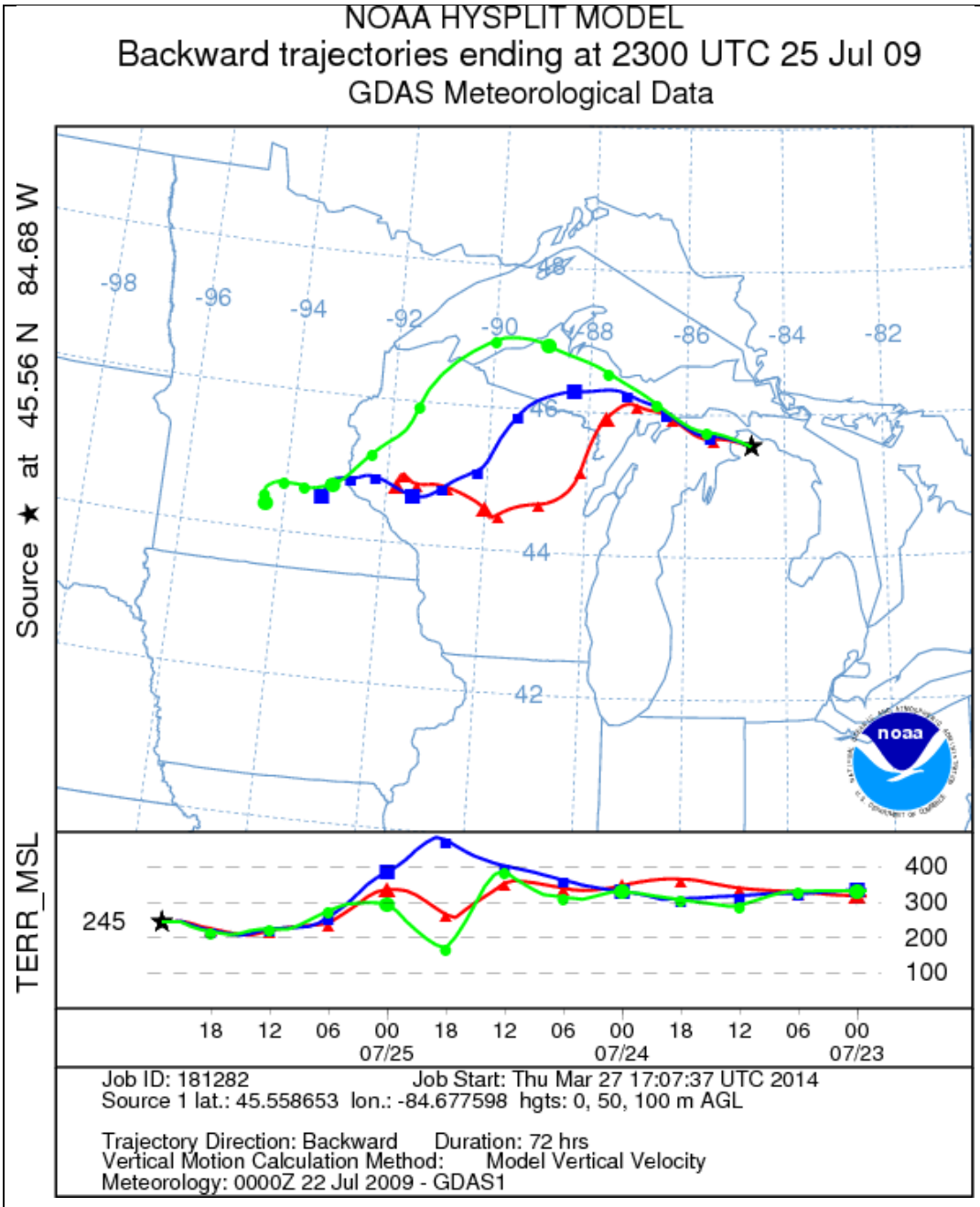
NOAA HYSPLIT MODEL
Backward trajectories ending at 2300 UTC 25 Jul 09
GDAS Meteorological Data
Source ★ at 45.56 N 84.68 W
TERR_MSL
-98
-96
-94
-92
-90
-88
-86
-84
-82
48
46
44
42
noaa
245
400
300
200
100
18 12 06 00 18 12 06 00 18 12 06 00
07/25
07/24
07/23
Job ID: 181282 Job Start: Thu Mar 27 17:07:37 UTC 2014
Source 1 lat.: 45.558653 lon.: -84.677598 hgts: 0, 50, 100 m AGL
Trajectory Direction: Backward Duration: 72 hrs
Vertical Motion Calculation Method: Model Vertical Velocity
Meteorology: 0000Z 22 Jul 2009 - GDAS1

a)

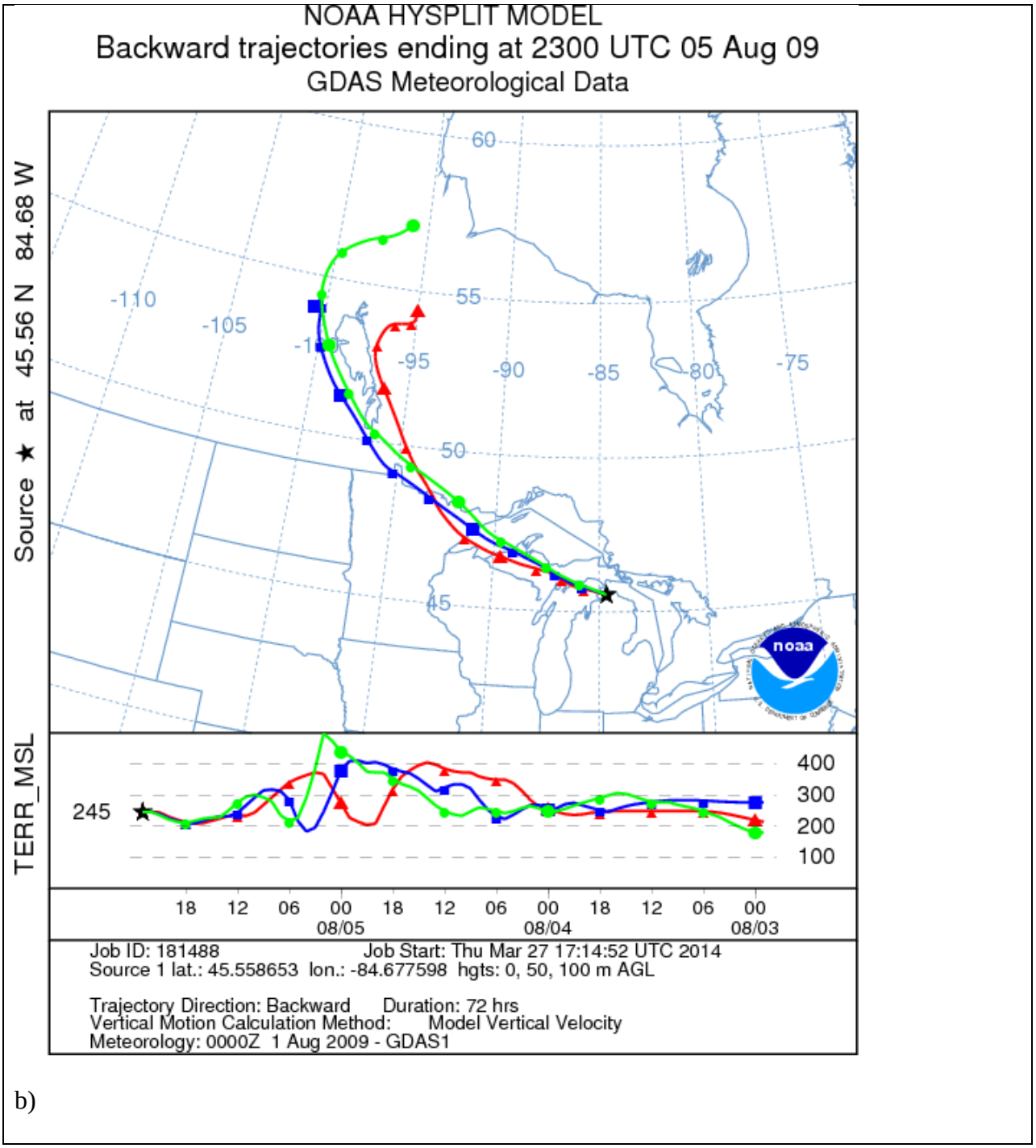
NOAA HYSPLIT MODEL
Backward trajectories ending at 2300 UTC 05 Aug 09
GDAS Meteorological Data
Source ★ at 45.56 N 84.68 W
TERR_MSL
60
55
50
45
-110
-105
-95
-90
-85
-80
-75
245
400
300
200
100
18 12 06 00 18 12 06 00 18 12 06 00
08/05
08/04
08/03
Job ID: 181488 Job Start: Thu Mar 27 17:14:52 UTC 2014
Source 1 lat.: 45.558653 lon.: -84.677598 hgts: 0, 50, 100 m AGL
Trajectory Direction: Backward Duration: 72 hrs
Vertical Motion Calculation Method: Model Vertical Velocity
Meteorology: 0000Z 1 Aug 2009 - GDAS1

b)

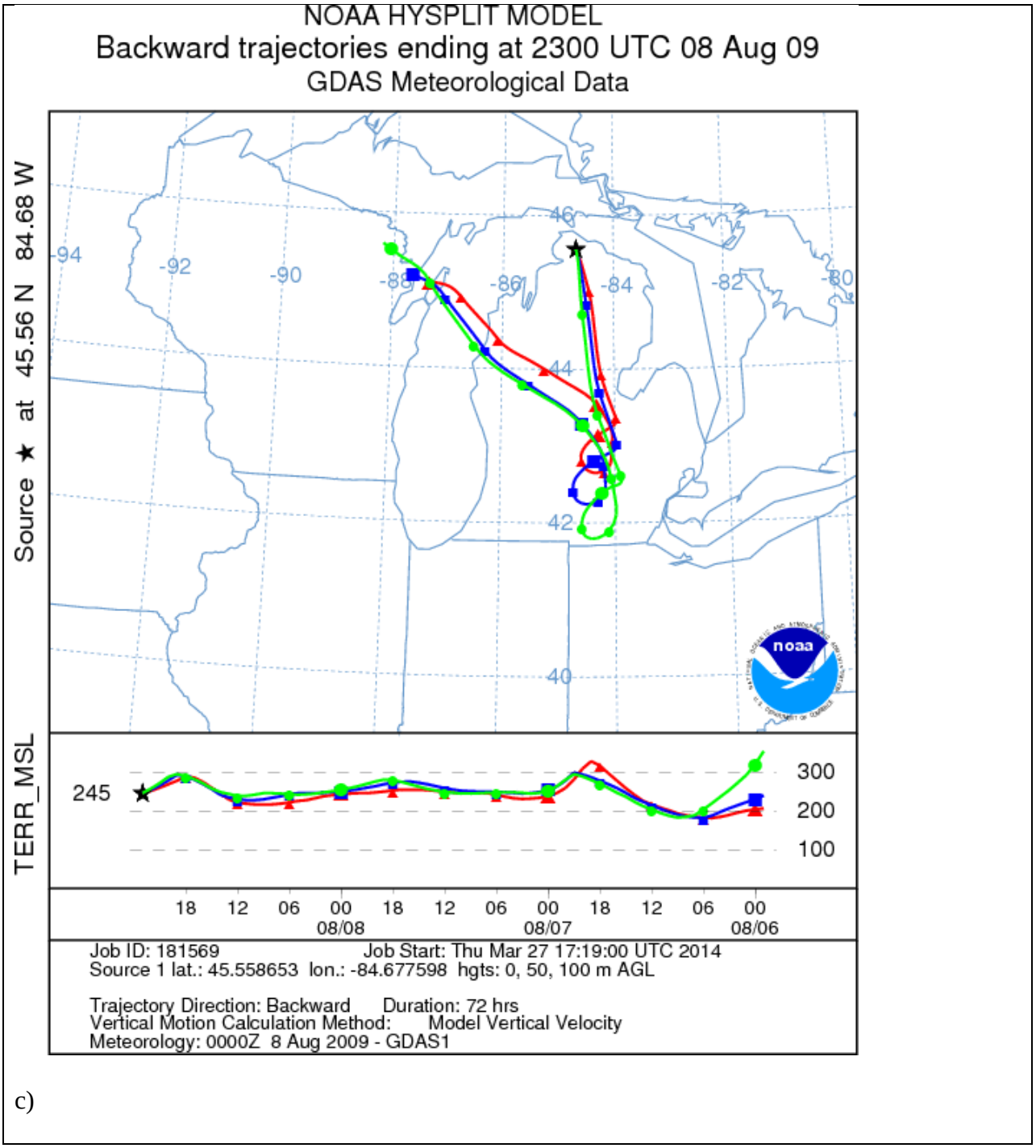

c)

Figure 11: NOAA HYSPLIT backward trajectory model predicting air parcel trajectories for air parcels arriving at Pelston at midnight a) July 25, 2009 b) August 05, 2009 c) August 08, 2009

Conclusion

Having few days with clear skies and little to no wind, in addition to poor instrument precision provided a difficult and challenging modeling case. There were problems with the LIF-FAGE laser, along with unidentified potential interferences. β-hydroxyperoxy radicals have been identified as a potential source of HO_2 measurement interferences (Da Silva et al., 2010). As all sources and types of instrumental errors have not been elucidated at the time of this writing a more detailed assessment of the model accuracy cannot be provided until a larger dataset can be obtained or algorithmic improvements to the current dataset are implemented. Further studies should be conducted to determine the instrumental contribution to systematic and random error.

Vehicle Indoor Air Quality Introduction

In today's modern motorized society, automobile cabins have become a part of the living environment. People are spending more time in their vehicles on the way to work, traveling for business or pleasure, shopping, and a multitude of motorized recreational activities. According to a recent ABC News/Time Magazine survey, 90 percent of Americans say they usually drive to work (Langer, 2005). McKenzie and Rapino report that 86.1% of the population they surveyed used a personal vehicle (car, truck, or van) or were part of a car pool and had a daily commute to and from work of approximately 50 minutes per day (McKenzie and Rapino, 2011). Those statistics do not take into consideration occupations where a presence is maintained in a vehicle cabin (e.g. taxi cab driver, freight driver, etc.), nor activities outside of getting to and from work. In addition, the average household owns one or two vehicles, 34.1% and 37.5% respectively, with 19.1% of the American population owning three or more vehicles (Davis et al., 2013).

The cabin can be considered to be an indoor space when the doors and windows are closed. Many organic compounds are present in indoor air, and exposure to them is one of the causes of the sick building syndrome. Specific VOCs and concentrations are not attributed to sick building syndrome (Brinke et al., 1998). In indoor environments someone is typically exposed to a hundred or more VOC's though at very low concentrations. As a result, vehicle cabins should be considered another potential source of "sick building syndrome". The symptoms of sick building syndrome have been described as fatigue, mental confusion, and acute discomfort, e.g., headache; eye, nose, or throat irritation; dry cough; dry or itchy skin; dizziness and nausea; difficulty in concentrating; fatigue; and sensitivity to odors (Indoor Air Facts, 1991). Sick building syndrome has not shown any detrimental effects on the performance of neurobehavioral tests (Otto et al., 1992).

Vehicle Contaminants

Yoshida et al. have surveyed 101 Japanese cars to establish the types and concentrations (2006b). This study involved cars that were from the model years 2001, 2002, 2003, and 2004 with 14, 28, 47, and 12 vehicles from those model years respectively. All vehicles were for private use in residential areas and stored in areas with low traffic volumes. Prior to sampling the vehicle was off for at least three hours with the windows, doors, and vents all shut. Yoshida et al. were able to detect 242 aromatic hydrocarbons in all the vehicles and a total of 275 observed VOC's. The median total VOC (TVOC) concentration, which is the sum of the interior concentrations of all quantitated compounds (except formaldehyde), was 601 $\mu g\ m^{-3}$, ranging from 136 $\mu g\ m^{-3}$ to 3968 $\mu g\ m^{-3}$. The partition of compounds in the measurements broke down as follows: aliphatic hydrocarbons, 74 (alkanes, 42; cycloalkanes, 24; alkenes, 6; cycloalkenes, 2); aromatic hydrocarbons, 50; halocarbons, 8; terpenes, 14; esters, 33; carbonyl compounds, 15

(aldehydes, 9; ketones, 6); other, 80 (alcohols and glycols, 30; quinones, 2; phenols, 4; ethers, 3; furans, 2; phosphates, 9; adipates, 3; phthalates, 11; nitrogen-containing compounds, 16) (Yoshida et al., 2006b). Yoshida's work did not speak to the outdoor level of these compounds. It is generally believed that indoor concentrations of many VOC's are greater than the local outdoor concentrations (Pellizzari et al., 1986; Chan et al., 1990; Hartwell et al., 1992; Pegas et al., 2011).

As the temperature inside vehicles rises so does the TVOC concentration, this is more pronounced in a vehicle cabin than in a residential or business dwelling. The diffusivity of the VOC's observed by Yoshida was investigated in an additional study. Of the 275 VOC's identified in the 101 vehicles, 162 VOC's were observed over the course of three years and their time course concentrations documented. The concentration of VOC's was seen to fluctuate seasonally with maximum VOC concentrations for all species observed during the summer and decreasing into the winter months. Over the three year study the maximum seasonal concentration of VOC's observed decreased (Yoshida and Matsunaga, 2006a).

VOC Toxicokinteics

With people spending 80%-90% of their time indoors, knowledge of the amounts of VOC's inhaled by vehicle occupants and the acute and chronic inhalation exposure is essential for evaluating the adverse effects on health. Knowledge of the inhalation toxicokinetics of a volatile substance is essential for understanding and extrapolating exposure dose–response relationships (Béliveau et al., 2005; Nong et al., 2005; Peyret and Krishnan, 2012). Yoshida has extrapolated the results from a toxicokinetic rat study and estimates that a person's two-hour presence in a vehicle cabin results in an estimated 30 µg absorption for toluene, 10 µg for ethylbenzene, 6 µg for o-xylene, 8 µg for m-xylene, 9 µg for p-xylene, 11 µg for styrene, and 27

µg for 1,2,4-trimethylbenzene, calculated per 60kg body weight (2010). This translates to percentage uptakes of 45%, 50%, 38%, 41%, 48%, 58%, 66% for toluene, ethylbenzene, *o*-xylene, *m*-xylene, *p*-xylene, styrene, and 1,2,4-trimethylbenzene, respectively (Yoshida, 2010). The tolerable daily intake (TDI) as suggest by the World Health Organization is 223 µg/kg body weight for toluene, 97.1 µg/kg body weight for ethylbenzene, 179 µg/kg body weight for xylenes, and 7.7 µg/kg styrene (2011).

New cars show greatly elevated levels of VOC's immediately after delivery (Filho, 2010; Yoshida et al., 2006b; Yoshida and Matsunaga, 2006a). The concentration of formaldehyde was found to be close to 50 µg m^{-3} in addition to the TVOC concentration being 1408 µg m^{-3} (Yoshida and Matsunaga, 2006a). The interior TVOC concentration decreases rapidly after delivery, coming to equilibrium after about six months. The interior concentration was the same level as the outdoor concentration in winter, but in summer, the interior concentration was elevated to concentrations greater than the observed outdoor concentration (Yoshida, 2010).

Current Guidelines

A guideline value of 300 µg m^{-3} by Seifert was proposed for the indoor concentration of TVOC (1995). Seven different chemical classes of VOC contributed to this value and their proposed indoor guideline values were as follows: alkanes, 100 µg/m3; aromatic hydrocarbons, 50 µg/m3; terpenes, 30 µg/m3; halocarbons, 30 µg/m3; esters, 20 µg/m3; carbonyl compounds (excluding formaldehyde), 20 µg/m3; other, 50 µg/m3. Besides this recommendation, no guidelines have been established for indoor air exposure to VOC's except formaldehyde. OSHA has established a guideline of limiting formaldehyde exposure per eight- hour interval to concentrations not greater than 0.75 ppm, which correlates to $8.175x10^{-5}$ µg m^{-3}. Only Japan (Ministry of Land, Infrastructure and Transportation Notification No. 2007-539), South Korea

(Notification No. 2007-539), and China (GB/T 27630-2011) have established guidelines for automobile manufactures, with many manufactures adhering to company standards (see Table 3). The Japan Automobile Manufacturers Association (JAMA) established a voluntary reduction of vehicle cabin VOC concentrations in 2007. The EPA does not currently consider vehicle cabins an indoor environment. They have provided no resources on vehicle cabin air quality. To aid in protecting commuter health and safety a standard should be established that most countries and all vehicle manufactures can abide by. This standard would also ease the vehicle manufacturing industry into compliance. This should be implemented before more countries establish proprietary regulations and manufactures create internal standards. Table 3 shows the guidelines followed by large automobile manufactures. It is clear these companies have their own regulatory guidelines for VOC concentration and testing and do not adhere to a common standard.

Table 3: VOC management status of several automobile manufactures.

Manufacturer	VOC regulations
Ford	VOC's regulated by Ford standard
GM	VOC's regulated by GM standard
Honda	Follows JAMA guidelines
Hyundai	Follows Korean guidelines
Jaguar Land-Rover	Applies both Korean and Chinese regulations
Kia	Follows Korean guidelines
Nissan	Follows JAMA guidelines and Nissan Global policy
Porsche	Follows German Automobile Industrial Association VDA 278 regulations
Toyota	Follows JAMA guidelines
Volvo	Follows Chinese regulations

Previous Studies

Beginning in 2003, Williams and Pharaoh began working in collaboration with Jaguar Land Rover, automotive suppliers, and additional partners to investigate vehicle interior air

quality. The goal of their eight-year study was to develop a system to insure the projected emission requirements in the UK can be met within the supply chain (2012). They have not published results from their work at the time of this writing but to date they have developed component and whole-vehicle test methodologies and are completing the initial round of materials evaluation and full-vehicle indoor air quality evaluations (Williams and Pharaoh, 2012).

Similarly the Society of Automotive Engineers (SAE) attempted to estimate the observable amounts of VOCs being emitted from products used in vehicles. Their strategy was to disassemble a vehicle, and using a sampling bag method, sum the total VOC emission piecewise based on the actual emission of VOC's from the individual components (Azuma et al., 2013). This method was not able to statistically reproduce measured vehicle emissions. The discrepancy between observed in-car and piecewise emission totals can be attributed to differing measurement conditions (temperature, volume of gas in sample bag used to acquire sample, etc…). It may also be a result of variance from within the supply chain or analytical technique as there were deviations in measured VOC emissions from the same sample, depending on the measurement conditions. In an attempt to improve their predictive ability utilizing a simple bag method a labeled compound was introduced. This enabled them to predict the amount of VOC contained in the material and the adsorptive capacity. This addition of a labeled compound yielded better results between the estimated and observed VOC emission totals (Iwai,et al., 2013).

Current Collaboration

It is difficult for manufacturers to identify potentially harmful VOC levels without extensive testing. As mentioned above, the measured emission rate of VOCs from a given source

is dependent on multiple factors that vary among laboratories. The Edwards group is developing a model which can be used during component development stages to help identify emission profiles, which is being expanded to model components in a vehicle cabin environment. In addition to modeling studies the Edwards group will be collaborating on the standardization by which emission profiles will be determined. A standardized reference material is being considered to reduce the inter-laboratory error and variability that exists when investigating emission profiles from materials (De Bortoli et al., 1999). The modeling studies performed herein in addition to emission inventories conducted elsewhere have been funded by the United States Council for Automotive Research LLC (USCAR) through the Environmental Regulatory Initiatives of Materials (ERIM). This work is in collaboration with Ford, General Motors, NIST, and Virginia Tech University. In future experiments, a small-scale chamber of $0.5\times0.4\times0.25$ m^3 will be used for measuring the component emissions in accordance with ASTM standard guide for small-scale environmental chamber determinations of organic emissions from indoor materials/products (ASTM D5116-10). The test conditions drafted by USCAR and NIST are as follows:

Table 4: USCAR-NIST draft procedure.

Temperature:	65 °C
Carrier Gas:	Air
Humidity:	0% Relative Humidity
Flow Rate	100 mL
Sorbent:	Tenax
Sample Time:	300 Minutes
Number of Samples per Reference:	10 Tubes
Number of Chamber Tests:	2
Compound loaded on reference material	Toluene – D8
Micro Chamber Size	4 gang, 250 mL

With the development of a standardized reference material that can be used for inter-laboratory studies, it is possible to begin the process of identifying and eliminating the root causes of variability in emissions testing (Cox et al., 2010; De Bortoli et al., 1999; De Bortoli and Colombo, 1993). In collaboration with the National Institute of Standards and Technology (NIST), researchers at Virginia Tech (VT) developed a reference material for VOC emissions testing. Polymethyl pentene (PMP), a thermoplastic polymer composed of 4-methy-1-pentene monomer units, has been studied intensively and found to closely resemble emissions from actual homogeneous building materials (Cox et al., 2010; Howard-Reed et al., 2011; Liu et al., 2013). The material-phase diffusion coefficient and the material/air interface exchange coefficient have been well documented and deemed suitable for an internal standard reference when loaded with deuterated toluene (Cox et al., 2010). Emissions of VOCs from these materials are largely controlled by internal diffusion. The effect of external convective mass transfer is negligible when the internal mass transfer resistance is large.

The initial focus of this research is twofold. First the reproducibility and correlation between the existing static and dynamic sampling will need to be tested. To do this it will be necessary to perform duplicate experiments involving the vehicle itself in addition to testing the emission rate of materials under various controlled regimes. The target molecules of this research will initially, be those previously identified in the literature (Chien, 2007; Yoshida *et at.*, 2006b) and/or that have been associated with specific materials such as upholstery or floor mats (Yoshida et al., 2006b). As this research progresses, the list will be expanded as necessary to include the identification of other molecules of interest. The goal is to obtain a VOC-specific emission algorithm to predict cabin VOC concentrations for a given set of control parameters (e.g. temperature and/or age of the vehicle as a whole, or the part undergoing testing). One of the goals of this proposal is to model such an algorithm for the VOC's of interest detected in previous studies. Exact knowledge of diffusion and partition coefficients and the initial concentrations are needed for VOC's of interest before a VOC-dependent algorithm can be established. For this reason a membrane system developed by Cox, and loaded with deuterated toluene, was used as an internal standard.

Model

The model was developed under the assumption that the material is a representative homogeneous medium (Little et al., 1994; Xu and Zhang, 2003; Deng and Kim, 2004). Mechanisms for the concentration-independent internal diffusion of VOCs within the material (characterized by the diffusion coefficient, D), partitioning between the material and the air at the material surface (described by an effective partition coefficient (K_v)), and the equilibrium partition coefficient between air and the chamber surface (K_s) were included. The sorption of VOCs onto the chamber walls was considered to be negligible because of the high volatility (and

therefore very low K_s). The material-phase concentration as a function of the distance from the base of the material and time is given by (Equation 12 (Little et al., 1994); $C(x,t)$ is the concentration of VOC in the material and x the distance from the base of the material. The thickness of the polymer (L), volumetric flow rate of clean air into the chamber (Q), volume of air in the chamber (V), polymer area (A) are all constrained by empirical observations. The parameter q_n is the positive roots of (Equation 16. The concentration of contaminant in the chamber air at any time, t, is obtained by substituting the concentration at the surface of the polymer slab into (Equation 13, where K_v is the linear partition coefficient. (Equation 13 is based on the assumption that equilibrium exists between VOC concentrations at the polymer surface and the chamber air.

$$C(x,t) = 2C_o \sum_{n=1}^{\infty} \left\{ \frac{e^{(-Dq_n^2 t)(h-kq_n^2)\cos(q_n x)}}{[L(h-kq_n^2)^2 + q_n^2(L+k) + h]\cos(q_n L)} \right\} \quad \text{(Equation 12)}$$

$$K_v = \frac{C|_{x=L}}{y} \quad \text{(Equation 13)}$$

$$h = \frac{(Q/A)}{(DK_v)} \quad \text{(Equation 14)}$$

$$k = \frac{(V/A)}{K_v} \quad \text{(Equation 15)}$$

$$q\tan(qL) = h - kq^2 \quad \text{(Equation 16)}$$

The influence of the model parameters on the resulting contaminant concentration in the chamber air is briefly examined. Inspection of (Equation 12) shows that the concentration in the air will be directly proportional to the initial concentration of the VOC in the material. Figure 12

and Figure 13 show the effect of variations in the diffusion and partition coefficients respectively, for an initial concentration of 9.11×10^{8} mg m^{-3}. Figure 12 shows plots of chamber air concentration for values of D varying between 0.1×10^{-12} and 10×10^{-12} m^2 s^{-1} at a constant K of 1000. Increasing the diffusion coefficient value results in higher emission rates at early times, and more rapid depletion of the VOC in the polymer slab. Figure 13 gives the emission profiles with K varying between 100 and 100,000 at a constant D of 1×10^{-12} m^2 s^{-1}. The influence of K is two-fold. First, increasing the K decreases the emission rate at early times and results in a slower depletion rate of the source, except for an anomaly when K has a value of 10,000. This anomaly is believed to be a result of the numerical method for finding the root of (Equation 16) diverging when the partition coefficient has a value of 10,000. This is not a current concern as the partition coefficient of deuterated toluene in the PMP sample is sub-100. The influence of a change in K is virtually insignificant below a value of about 1,000. On the other hand, it was observed that although the initial emission and depletion rates vary significantly for different K, the chamber concentration after some time is almost identical. This suggests that for a dry source with small diffusivity, K may only affect early-stage emissions. However, the influence of a change in K is virtually insignificant below a value of about 1000.

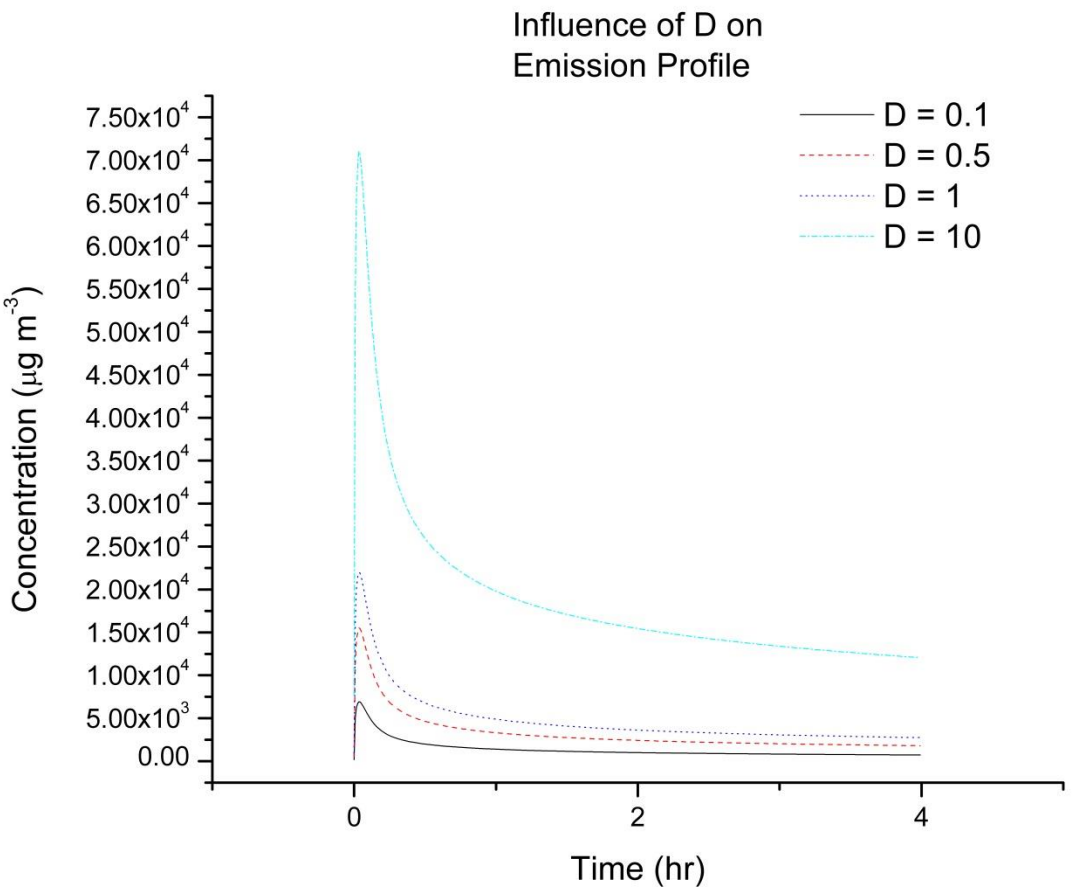

Figure 12: Influence of diffusion coefficient on emission profile

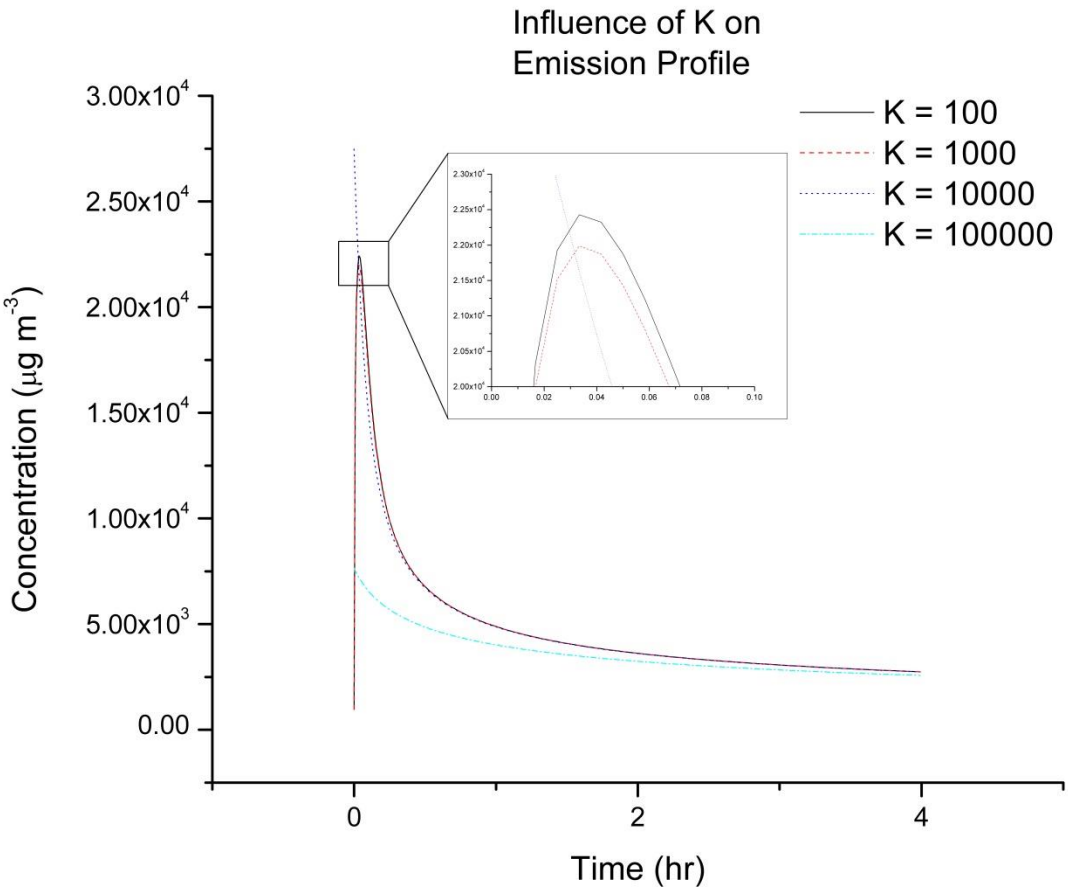

Figure 13: Influence of partition coefficient on emission profile.

Figure 14 shows the emission profile as predicted by the model, constrained by chamber and sample characteristics (L, A, Q, and V) and variable mass-transfer properties (K, D, and C0). Mass transfer properties of the toluene-loaded PMP film were provided by Steven Cox and USCAR.

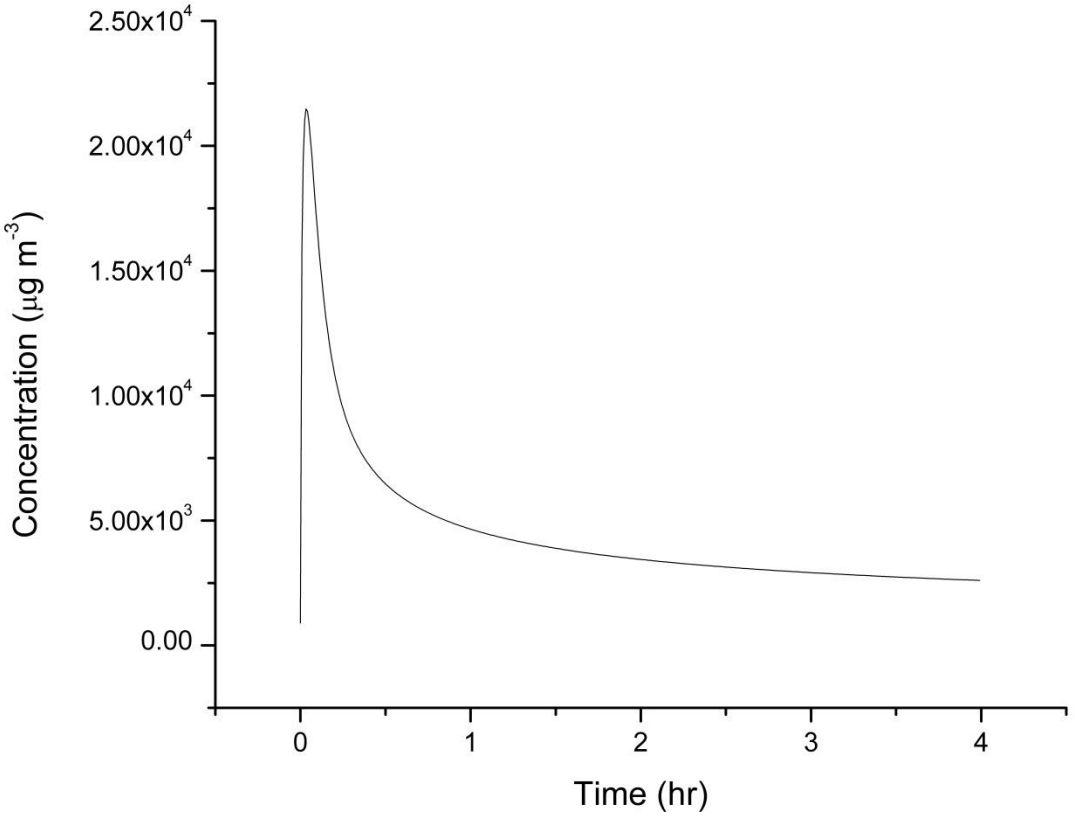

Figure 14: Chamber emission model prediction

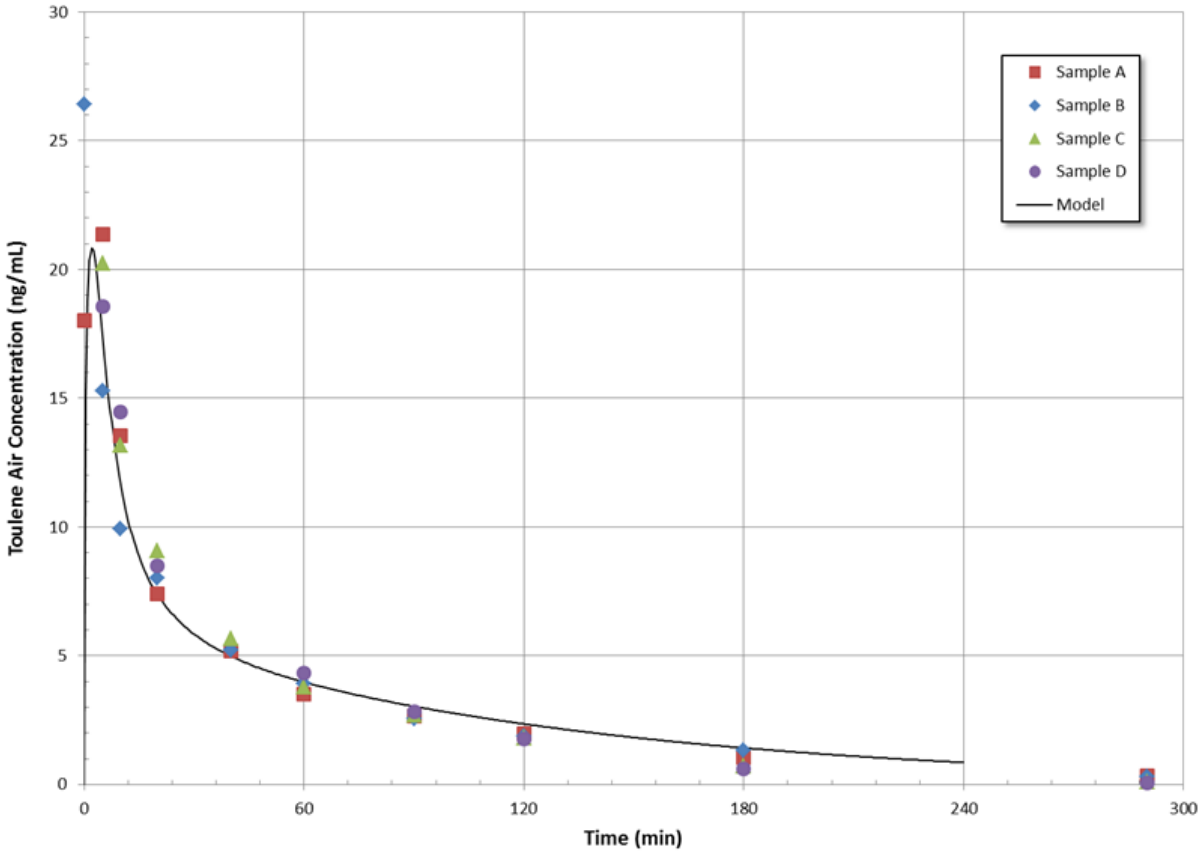

Figure 15: Results from NIST desorption studies

Figure 15 shows a comparison of observed to predicted toluene emission chamber results conducted by NIST. Eight PMP samples were tested over two days immediate after receipt of the samples. Two sets of micro-chamber desorption experiments were performed each day using four PMP samples. Two samples were used for micro-chamber desorption analysis. The other two PMP samples were used to determine the initial concentration. This was performed in duplicate.

The model is transitioning from an under prediction to an over prediction, indicating that the diffusion coefficient is likely too low for the chamber tests and further analysis is needed.

Because of the low value for D this model doesn't account for external mass transfer. Currently it is assumed that all emissions into the chamber air instantaneously well mixed. Until more research is conducted to reevaluate the diffusivity coefficient of toluene in the PMP films, external mass transfer will be omitted. When VOCs with larger D values are used, or when different emission materials are considered, the external mass transfer may play a significant role. This is obvious as transport between two phases requires a departure from equilibrium, and with relatively low values for D, this change in equilibrium is negligible.

Future Work

Deng and Kim have further improved Little's model with the inclusion of the external mass transfer (2004). The concentration in the air as described by Deng and Kim is given in (Equation *17*, where q_n is again the positive roots of (Equation 19, and β is the ratio of the material to air (vol/vol). (Equation 18) describes A_n, a coefficient where α is the dimensionless air exchange rate, Bi_m is the Biot number for mass transfer. The Biot number is defined by the previously-omitted mass transfer coefficient multiplied by the material thickness divided by the diffusion coefficient as shown in (Equation 20. The Biot number gives the ratio of the mass transfer resistance inside of and at the surface of a system. This ratio determines whether or not the concentration inside a system will vary significantly in space from a concentration gradient applied to its surface. Problems involving Biot numbers much smaller than 1, due to the uniformity of the concentration gradient in the system, are simple as the internal resistance to mass transfer can be neglected and the mass transfer process can be described by a lumped parameter model. Biot numbers much larger than 1 are indicative of non-uniformity in the concentration gradient within the object, and thus the internal resistance to mass transfer cannot

be neglected. In the Deng and Kim set of equations δ represents the material thickness, N the air exchange rate, and h the gas-phase mass transfer coefficient.

$$C_a(t) = 2C_0\beta \sum_{n=0}^{\infty} \frac{q_n \sin(q_n)}{A_n} e^{-D\beta^{-2}q_n^2 t} \quad \text{(Equation 17)}$$

$$A_n = [k\beta + (\alpha - q_n^2)kBi_m^{-1} + 2]q_n^2 \cos(q_n) + q_n \sin(q_n)[k\beta + (\alpha - 3q_n^2)kBi_m^{-1} + \alpha - q_n^2] \quad \text{(Equation 18)}$$

$$q_n \tan(q_n) = \frac{\alpha - q_n^2}{k\beta + (\alpha - q_n^2)kBi_m^{-1}} \quad \text{(Equation 19)}$$

$$Bi_m = \frac{h\delta}{D} \quad \text{(Equation 20)}$$

$$\alpha = \frac{N\delta^2}{D} \quad \text{(Equation 21)}$$

$$\beta = L\delta \quad \text{(Equation 22)}$$

As this work progresses further, the current model for predicting VOC emission from materials will be developed toward the representation of a production vehicle. Evaluations for individual substances can be made on the basis of defined criteria as illustrated above, but in the case of mixtures of substances or particles, as is observed in production vehicles, the problem of possible synergistic effects arises. The model will be adaptable for a multitude of VOC's and in time will be able to solve for them simultaneously. This could be accomplished by looping the code over several different inputs generating time course emission data for several species of interest. That output data can then be combined and used as input into a numerical integration suite such as FACSIMILE. This model could then be used before a vehicle enters the production

stage, to estimate the air quality within the cabin and ascertain as to whether or not it will meet the governing standards.

The material described herein has been highly positive *per se* as a model was developed that correlated with internally valid predictions, i.e. predictions that are valid for measurements constrained to the 2009 CABINEX field campaign, and for the insight into the main causes and sources of errors and inconsistencies in atmospheric modeling. For the first time the interior VOC concentrations of a vehicle are being investigated via mass transfer modeling in conjunction with the use of a standardized emission source. The results are particularly useful considering the multitude of standards VOC analysis standards in practice, and the variability observed between inter-laboratory studies.

References

Amedro, D; Miyazaki, K.; Parker, A.; Schoemaecker, C.; Fittschen, C. Atmospheric and kinetic Studies of OH and HO_2 by the FAGE Technique. *Journal of Environmental Sciences,* **2012,** 24, 78-86.

Atkinson, R. Estimation of OH Radical Reaction Rate Constants and Atmospheric Lifetimes for Polychloroblphenyls, Dibenzo-p-dioxins, and Dibenzofurans. *Environ. Sci. Technol.,* **1987,** *21*, 305-307.

Atkinson, R.; Baulch, D.; Cox, R.; Crowley, J.; Hampson, R.; Hynes, R.; Jenkin, M.; Rossi, M.; Troe, J. Evaluated kinetic and photochemical data for atmospheric chemistry: Volume I – gas phase reactions of Ox, HOx, NOx and SOx species. *Atmos. Chem. Phys.*, **2004,** *4*, 1461–1738,

Atkinson, R.; Baulch, D.; Cox, R.; Crowley, J.; Hampson, R.; Hynes, R.; Jenkin, M.; Rossi, M.; Troe, J.; IUPAC Subcommittee. Evaluated kinetic and photochemical data for atmospheric chemistry: Volume II - gas phase reactions of organic species. *Atmos. Chem. Phys.*, **2006,** *6*, 3625–4055.

Azuma, M.; Kubo, H.; Amari, A.; Iwai, K.; Hayakawa, K.; Motoyama, Y.; Ito, H.; Imaeda, T. *Study on the Prediction of VOC Concentration in Vehicle Cabins (1) Investigation of Relationship between Toluene Concentrations and Evaluation Conditions using Interior Parts;* 2013-01-0490; SAE: 2013.

Barket, D.; Hurst, J.; Couch, T.; Colorado, A.; Shepson, P.; Riemer, D.; Hills, A.; Apel, E.; Hafer, R.; Lamb, B.; Westberg, H.; Farmer, C.; Stabenau, E.; Zika, R. Intercomparison of automated methodologies for determination of ambient isoprene during the PROPHET 1998 summer campaign. *J. Geophys. Res.*, **2001,** *106*, 24301-24313.

Bauer, D.; D'Ottone, L.; and Hynes, A. O(^{1}D) Quantum Yield from Ozone Photolysis in the Near UV Region Between 305 and 375nm, *J. Phys. Chem.*, **2000,** *2*, 1421-1424.

Béliveau, M.; Lipscomb, J.; Tardif, R.; Krishnan, K. Quantitative Structure−Property Relationships for Interspecies Extrapolation of the Inhalation Pharmacokinetics of Organic Chemicals. *Chem. Res. Toxicol.*, **2005,** *18*, 475-485.

Bernhardson, C. Type I Error Rates When Multiple Comparison Procedures Follow a Significant F Test of ANOVA. *Biometrics*, **1975,** *31*, 229-232.

Bloss, W.; Camredon, M.; Lee, J.; Heard, D.; Plane, J.; Saiz-Lopez, A.; Bauguitte, S.; Salmon, R. Coupling of HO_x, NO_x and halogen chemistry in the Antarctic boundary layer. *Atmos. Chem. Phys.*, **2010,** *10*, 10187-10209.

Brinke, J.; Selvin, S.; Hodgson, A.; Fisk, W.; Mendell, M.; Koshland, C.; Daisey, J. Development of New Volatile Organic Compound (VOC) Exposure Metrics and their Relationship to "Sick Building Syndrome" Symptoms. *Indoor Air*, **1998,** *8*, 140-152.

Bryan, A.; Bertman, S.; Carroll, M.; Dusanter, S.; Edwards, G.; Forkel, R.; Griffith, S.; Guenther, A.; Hansen, R.; Helmig, D.; Jobson, B.; Keutsch, F.; Lefer, B.; Pressley, S.; Shepson, P.; Stevens, P.; Steiner, A. In-canopy gas-phase chemistry during CABINEX 2009: sensitivity of a 1-D canopy model to vertical mixing and isoprene chemistry. *Atmos. Chem. Phys.*, **2012,** *12*, 8829-8849.

Carpenter, L.; Green, T.; Mills, G.; Bauguite, S.; Penkett, S.; Zanis, P.; Scheupbach, E.; Schmidbauer, N.; Monks, P.; Zellweger, C. Oxidized Nitrogen and Ozone Production Efficiencies in the Springtime Free Troposphere over the Alps. *J. Geophys. Res.*, **2000,** 549-559.

Carroll, M.; Bertman, S.; Shepson, P. Overview of the Program for Research on Oxidants: PHotochemistry, Emissions, and Transport (PROPHET) summer 1998 measurements intensive. *J. Geophys. Res.*, **2012,** *106*, 24275–24288.

Carslaw, N.; Creasey, D.; Heard, D.; Lewis, A.; Monks, P.; Bandy, B.; Penkett, S. Modelling OH, HO2, and RO2 Radicals in the Marine Boundary Layer: Model Construction and Comparison with Field Measurements. *J. Geophys. Res.*, **1999,** *104*, 241-255.

Carter, W. and Atkinson, R. Development and evaluation of a detailed mechanism for the atmospheric reactions of isoprene and NO_x, *Int. J. Chem. Kinet.*, **1996,** *28*, 497-530.

Chan, C.; Vainer, L.; Martin, J.; Williams, D. Determination of organic contaminants in residential indoor air using an adsorption–thermal desorption technique, *J. Air. Waste. Manage. Assoc.*, **1990,** *40*, 62–7.

Chapman, S. A theory of upper atmospheric ozone. *Mem. Roy. Meteor. Soc.* **1930,** *3*, 103–125.

Chien, Y. Variations in amounts and potential sources of volatile organic chemicals in new cars. *Sci. Total Environ.*, **2007,** *382*, 228-239.

Crawford, J.; Davis, D.; Chen, G.; Bradshaw, J.; Sandholm, S.; Kondo, Y.; Liu, S.; Browell, E.; Gregory, G.; Anderson, B.; Sachse, G.; Collins, J.; Barrick, J.; Blake, D.; Talbot, R.; Singh, H. An Assessment of Ozone Photochemistry in the Extratropical Western North Pacific: Impact of Continental Outflow During Late Winter/Early Spring. *J. Geophys. Res.*, **1997,** *102*, 469-487.

Creasey, D.; Evans, G.; Heard, D.; Lee, J. Measurements of OH and HO_2 concentrations in the Southern Ocean marine boundary layer. *J. Geophys. Res.*, **2003,** *108*, 4775-4787.

Curtis, A. and Sweetenham, W. FACSIMILE/CHEKMAT User's Manual, AERER12805, London, HMSO, **1987.**

Da Silva, G.; Graham, C.; Wang, Z. Unimolecular β-Hydroxyperoxy Radical Decomposition with OH Recycling in the Photochemical Oxidation of Isoprene. *Environ. Sci. Technol.*, **2010,** *44*, 250-256.

Davis, S.; Diegel, S.; Boundy, R. Household Vehicles and Characteristics. *Transportation Energy Data Book*, 32; U.S. Department of Energy: Washington, DC, 2013.

De Bortoli, M. and Colombo, A. Interlaboratory comparison of small chamber measurements. *Determination of VOCs e from indoor materials and products*; Report No. 13; Commission of the European Communities Joint Research Centre, Environment Institute: Ispra, Italy, 1993.

De Bortoli, M.; Kephalopoulos, S.; Kirchner, S.; Schauenburg, H.; Vissers, H. State-of-the-Art in the Measurement of Volatile Organic Compounds Emitted from Building Products: Results of European Interlaboratory Comparison. *Indoor Air*, **1999,** *9*, 103-116.

DeMore, W. G.; Sander, S. P.; Golden, D. M.; Hampson, R. F.; Kurylo, M. J.; Howard, C. J.; Ravishankara, A. R.; Kolb, C. E.; and Molina, M. J. *Chemical Kinetics and Photochemical Data for Use in Stratospheric Modeling*; Evaluation No. 12, JPL Publication 97-4. Jet Propulsion Laboratory, Pasadena, CA., 1997.

Deng, B. and Kim, C. An analytical model for VOCs emission from dry building materials. *Atmos. Environ.,* **2004,** *38*, 1173-1180.

Draxler, R.R. and Rolph, G.D., 2013. HYSPLIT (HYbrid Single-Particle Lagrangian Integrated Trajectory) Model access via NOAA ARL READY Website (http://www.arl.noaa.gov/HYSPLIT.php). NOAA Air Resources Laboratory, College Park, MD.

Dusanter, S.; Vimal, D.; Stevens, P. Technical note: Measuring tropospheric OH and HO_2 by laser-induced fluorescence at low pressure. A comparison of calibration techniques. *Atmos. Chem. Phys.*, **2008,** *8*, 321–340.

Dusanter, S.; Vimal, D.; Stevens, P.; Volkamer, R.; Molina, L. Measurements of OH and HO_2 concentrations during the MCMA-2006 field campaign – Part 1: Deployment of the Indiana University laser-induced fluorescence instrument. *Atmos. Chem. Phys.,***2009a,** *9*, 1665–1685.

Dusanter, S.; Vimal, D.; Stevens, P.; Volkamer, R.; Molina, L.; Baker, A.; Meinardi, S.; Blake, D.; Sheehy, P.; Merten, A.; Zhang, R.; Zheng, J.; Fortner, E.; Junkermann, W.; Dubey, M.; Rahn, T.; Eichinger, B.; Lewandowski, P.; Prueger, J.; Holder, H. Measurements of OH and HO_2 concentrations during the MCMA-2006 field campaign – Part 2: Model comparison and radical budget. *Atmos. Chem. Phys.,* **2009b,** *9*, 6655-6675.

Edwards, G. Aircraft Studies of Atmospheric Chemistry Over the North Atlantic. Ph.D. Dissertation, University of Leicester, Leicester, United Kingdom, 2000

Filho, A. *New Vehicles Cabin Indoor Air Quality*; SAE Technical Paper 2010-36-0390, 2010

Finlayson-Pitts, B.; Pitts, J. Tropospheric Air Pollution: Ozone, Airborne Toxics, Polycyclic Aromatic Hydrocarbons, and Particles. *Science (Washington, DC, U.S.),* **1997,** *276*, 1045-1051.

Fonton, M. Clouds, Sounding Balloons and Stratosphere; Teisserenc de Bort: a life in Meteorology

Goldstein, A.; Fan, S.; Goulden, M.; Munger, J.; Wofsy, S. Emission of Ethene, Propene, and 1-Butene by a Midlatitude Forest. *J. Geophys. Res.*, **1996,** *101*, 9149-9157.

Griffith, S.; Hansen, R.; Dusanter, S.; Stevens, P.; Alaghmand, M.; Bertman, S.; Carroll, M.; Erickson, M.; Galloway, M.; Grossberg, N.; Hottle, J.; Hou, J.; Jobson, B.; Kammrath, A.; Keutsch, F.; Lefer, B.; Mielke, L.; O'Brien, A.; Shepson, P.; Thurlow, M.; Wallace, W.; Zhang, N.; Zhou, X. OH and HO_2 radical chemistry during PROPHET 2008 and CABINEX 2009 – Part 1: Measurements and model comparison. *Atmos. Chem. Phys.*, **2013,** 5403-5423.

Guide for Small-Scale Environmental Chamber Determinations of Organic Emissions from Indoor Materials/Products. ASTM, West Conshohocken, PA, **2010**

Hanna, S.; Chang, J.; Fernau, M. Monte Carlo Estimates of Uncertainties in Predictions by a Photochemical Grid Model (UAM-IV) Due to Uncertainties in Input Variables. *Atmos. Environ.* **1998,** *32*, 3619–3628.

Hard, T.; George, L.; O'Brien, R. FAGE Determination of Tropospheric HO and HO2. *J. Atmos. Sci.*, **1995,** 52, 3354-3372.

Hard, T.; O'Brien, R.; Chan, C.; Mehrabzadeh, A. Tropospheric Free Radical Determination by FAGE. *Environ. Sci. Technol.* **1984,** *18*, 768-777.

Hartwell, T.; Perritt, R.; Pellizzari, E.; Michael, L. Results from the 1987 total exposure assessment methodology (TEAM) study in southern California. *Atmos. Environ.*, **1992**, *26A*, 1519–27.

Hintsa, E.; Boering, K.; Weinstock, E.; Anderson, J.; Grey, B.; Pfister, L.; Daube, B.; Wofsy, S.; Loewenstein, M.; Podolske, J.; Margitan, J.; and Bui, T. Troposphere-to-stratosphere transport in the lowermost stratosphere from measurements of H_2O, CO_2, N_2O and O_3, *Geophys. Res. Lett.* **1998,** 2655-2658.

Hofmann, U.; Weller, D.; Ammann, C.; Jork, E.; and Kesselmeier, J.: Cryogenic trapping of atmospheric organic acids under laboratory and field conditions, *Atmos. Environ.* 1997 **31,** 1275-1284.

Hofzumahaus, A.; Rohrer, F.; Lu, K.; Bohn, B.; Brauers, T.; Chang, C.; Fuchs, H.; Holland, F.; Kita. K.; Kondo, Y.; Li, X.; Lou, S.; Shao, M.; Zeng, L.; Wahner, A.; Yuanhang, Z. Amplified Trace Gas Removal in the Troposphere. *Science (Washington, DC, U.S.),* **2009,** *324*, 1702-1704.

Holton, J.; Haynes, P.; McIntyre, M.; Douglass, A.; Rood, R.; Pfister, L. Stratosphere-Troposphere Exchange. *Rev. of Geophys.* **1995,** *33*, 403-439.

Indoor Air Facts No. 4 Sick Building Syndrome; Research and Development MD-56; United States Environmental Protection Agency: 1991; 1-4.

International Organization for Standardization, Standard Atmosphere, ISO 2533:1975, 1975.

Iwai, K.; Hayakawa, K.; Motoyama, Y.; Ito, H.; Imaeda, T.; Azuma, M.; Kubo, H.; Amari, A. *Study on the Prediction of VOC Concentration in Vehicle Cabins (2) Development of Labeled Compound Addition Method;* 2013-01-0491, SAE: 2013.

Japan Automobile Manufacturers Association. JAMA Announces Voluntary Guidelines for Reducing Vehicle Cabin VOC Concentration Levels [Press release]. 2005. Retrieved from http://www.jama-english.jp/release/release/2005/050214.html

Jenkin, M.; Saunders, S.; Pilling, M. The tropospheric degradation of volatile organic compounds: A protocol for mechanism development. *Atmos. Environ.*, **1997,** *31*, 81-104.

Jones, a. E.Butler, T.; Taraborrelli, D.; Brühl, C.; Fischer, H.; Harder, H.; Martinez, M.; Williams, J.; Lawrence, M.; Lelieveld, J. Improved simulation of isoprene oxidation chemistry with the ECHAM5/MESSy chemistry-climate model: lessons from the GABRIEL airborne field campaign. *Atmos. Chem. Phys.*, **2008,** *8*, 4529-4546.

Kesselmeier, J.; Staudt, M. Biogenic Volatile Organic Compounds (VOC): An Overview on Emission, Physiology and Ecology. *J. Atmos. Chem.*, **1999,** *33*, 23-88.

Kiel, J.; Trenberth, K. Earth's Annual Global Mean Energy Budget. Bull. Am. Meteorol. Soc. 78, 197-208.

Kirchner, F.; Jeanneret, F.; Clappier, A.; Krüger B.; Bergh, H.; and Calpini, B. Total VOC reactivity in the planetary boundary layer 2. A new indicator for determining the sensitivity of the ozone production to VOC and NO_x. *J. Geophys. Res.*, **2001,** *106*, 3095-3110.

Klem, O.; Stockwell, W.; Schlager, H.; Krautstrunk, M. NO_x or VOC Limitation in East German Ozone Plumes? *J. Atms. Chem.*, **2000,** *35*, 1-18.

Kubistin, D.; Harder, H.; Martinez, M.; Rudolf, M.; Sander, R.; Bozem, H.; Eerdekens, G.; Fischer, H.; Gurk, C.; Klüpfel, T.; Königstedt, R.; Parchatka, U.; Schiller, C.; Stickler, A.; Taraborrelli, D.; Williams, J.; Lelieveld, J. Hydroxyl radicals in the tropical troposphere over the Suriname rainforest: comparison of measurements with the box model MECCA. *Atmos. Chem. Phys.*, **2010,** *10*, 9705-9728.

Langer, G. Poll: Traffic in the United States. *ABC News* [online] **2005.** http://abcnews.go.com/Technology/Traffic/story?id=485098&page= (accessed June 26, 2013)

Lelieveld, J.; Butler, T.; Crowley, J.; Dillon, T.; Fischer, H.; Ganzeveld, L.; Harder, H.; Lawrence, M.; Martinez, M.; Taraborrelli, D.; Williams, J. Atmospheric oxidation capacity sustained by a tropical forest. *Nature*, **2008,** *452*, 737-40

Little, J.; Hodgson, A.; Gadgil, A. Modeling Emissions of Volatile Organic Compounds from New Carpets. *Atmos. Environ.*, **1994,** *28*, 227-234.

Logan, J.; Prather, M.; Wofsy, S.; McElroy, M. Tropospheric Chemistry: A Global Perspective. *J. Geophys. Res.,* **1981,** *86*, 7210-7254.

Mandronich, S. Photodissociation in the Atmosphere 1. Actinic Flux and the Effects of Ground Reflections and Clouds. *J. Geophys. Res.,* **1987,** *92*, 9740-9752.

Madronich, S. and Flocke, S.: The role of solar radiation in atmospheric chemistry, in: Handbook of Environmental Chemistry, edited by: Boule, P., 1–26, Springer, NewYork, USA, 1998.

Madronich, S.; Weller, G. Numerical-integration errors in calculated tropospheric photodissociation rate coefficients. *J. Atmos. Chem.,* **1990,** *10*, 289–300.

Monks, P., Carpenter, L., Penkett, S., & Ayers, G. Night-time peroxy radical chemistry in the remote marine boundary layer over the Southern ocean. *Geophysical Research Letters*, **1996,** *23*, 535–538.

Moody, J. and Samson, P. The influence of atmospheric transport on the composition of precipitation at two sites in the Midwestern United States. *Atmos. Environ.,* **1989,** *23*, 2117-2132.

McKenzie, B. and Rapino, M. *Commuting in the United States: 2009;* American Community Survey Reports, ACS-15; U.S. Census Bureau: Washington, DC, 2011.

NARSTO. An Assessment of Tropospheric Ozone Pollution. **2000,** Richland, WA, NARSTO

Nong, A.; Charest-Tardif, G.; Tardif, R.; Lewis, D.; Sweeney, L.; Gargas, M.; Krishnan, K. Physiologically based modeling of the inhalation pharmacokinetics of ethylbenzene in B6C3F1 mice. *J. Toxicol. Environ. Health,* **2007,** *70*, 1838-1848.

OriginPro, OriginLab, Northampton, MA

Otto, D.; Hudnell, H.; House, D.; Mølhave, L.; Counts, W. Exposure of humans to a volatile organic mixture. I. Behavioral assessment. *Arch. Envriron. Health,* **1992,** *47*, 23-30.

Paulson, S.; Seinfeld, J. Development and evaluation of a photooxidation mechanism for isoprene, *J. Geophys. Res.,***1992,** *97*, 20703-20715.

Paulson, S., Flagan, R., and Seinfeld, J. Atmospheric photooxidation of isoprene Part I: The hydroxyl radical and ground state oxygen reactions, *Int. J. Chem. Kinet.,* **1992a,** *24*, 79-101.

Paulson, S., Flagan, R., and Seinfeld, J. Atmospheric photooxidation of isoprene Part II: The ozone-isoprene reaction, *Int. J. Chem. Kinet.,* **1992b,** *24*, 103-125.

Pegas, P.; Alves, C.; Evtyugina, M.; Nunes, T.; Cerqueira, M.; Franchi, M.; Pio, C.; Almeida, S.; Cabo Verde, S.; Freitas, M. Seasonal evaluation of outdoor/indoor air quality in primary schools in Lisbon, *J. Environ. Monit.,* **2011,** *13*, 657-667.

Pellizzari, E.; Hartwell, T.; Perritt, R.; Sparacino, C.; Sheldon, L.; Zelon, H.; Whitmore, R.; Breen, J.; Wallace, L. Comparison of Indoor and Outdoor Residential Levels of Volatile Organic Chemicals in Five U.S. Geographical Areas, *Environ. Int.,* **1986.** *12*, 619-623.

Peyret, T. and Krishnan, K. Quantitative Property-Property Relationship for Screening-Level Prediction of Intrinsic Clearance of Volatile Organic Chemicals in Rats and Its Integration within PBPK Models to Predict Inhalation Pharmacokinetics in Humans. *J. Toxicol.*, **2012,** *2012*, 1-22.

Pressley, S.; Lamb, B.; Westberg, H.; Flaherty, J.; Chen, J. Long-term isoprene flux measurements above a northern hardwood forest. *J. Geophys. Res.*, **2005,** *110*, D07301.

Ravishankara, A.; Solomon, S.; Turnipseed, A.; Warren, R. Atmospheric Lifetimes of Long-Lived Halogenated Species. *Science (Washington, DC, U.S.)*, **1993,** *259*, 194-199.

Ren, X.; Brune, W.; Oliger, A.; Metcalf, A.; Simpas, J.; Shirley, T.; Schwab, J.; Bai, C.; Roychowdhury, U.; Li, Y.; Cai, C.; Demerjian, K.; He, Y.; Zhou, X.; Gao, H.; Hou, J. OH, HO_2 , and OH reactivity during the PMTACS–NY Whiteface Mountain 2002 campaign: Observations and model comparison. *J. Geophys. Res.*, **2006,** *111*, D10S03.

Rolph, G.D., 2013. Real-time Environmental Applications and Display sYstem (READY) Website (http://www.ready.noaa.gov). NOAA Air Resources Laboratory, College Park, MD.

Sander, S.; Friedl, R.; Abbatt, J.; Barker, J.; Burkholder, J.; Golden, D.; Kolb, C.; Kurylo, M.; Moortgat, G.; Wine, P.; Huie, R.; Orkin, V. Chemical Kinetics and Photochemical Data For Use in Atmospheric Studies. Evaluation Number 17, National Aeronautics and Space Administration, Jet Propulsion Laboratory, JPL Publication 10-6, **2011.**

Sawyer, R.; Harley, R.; Cadle, S. Mobile Sources Critical Review: NARSTO Assessment. *Atmos. Environ.*, **2000,** *34*, 2161-2281.

Seifert, B. Volatile organic compounds. In *Indoor air quality: A comprehensive reference book*; Maroni, M., Seifert, B., Lindvall, T., Eds.; Air quality monographs ; Elsevier Science: New York, 1995; vol. 3, 819–821.

Seinfeld. J.; Pandis, S. Atmospheric Chemistry And Physics, 2nd ed.; Wiley: Hoboken, 2006; pp 4-6.

Statistics Canada. www12.statcan.ca (accessed Mar 13, 2013).

Stone, D.; Evans, M.; Commane, R.; Ingham, T.; Floquet, C.; McQuaid, J.; Brookes, D.; Monks, P.; Purvis, R.; Hamilton, J.; Hopkins, J.; Lee, J.; Lewis, A.; Stewart, D.; Murphy, J.; Mills, G.; Oram, D.; Reeves, C.; Heard, D. HO_x observations over West Africa during AMMA: impact of isoprene and NO_x, *Atmos. Chem. Phys.*, **2010,** *10*, 9415-9429.

United States Census Bureau. http://quickfacts.census.gov (accessed Mar 13, 2013).

U.S. Standard Atmosphere, 1976; U.S. Government Printing Office, Washington, D.C., 1976

Westberg, H.; Lamb, B.; Hafer, R.; Hills, A.; Shepson, P.; Vogel, C. Measurement of isoprene fluxes at the PROPHET site, *J. Geophys. Res.*, **2012,** *106*, 24347–24358.

Williams, G. and Pharaoh, M. Vehicle Interior Air Quality, 2012. http://www2.warwick.ac.uk/fac/sci/wmg/research/pard/pardprojects/viaq/ (accessed May 23, 2013)

World Health Organization. 2011. Guidelines for Drinking-water Quality. Fourth edition. WHO: Geneva

Xu, Y. and Zhang Y. An improved mass transfer based model for analyzing VOC emissions from building materials. *Atmos. Environ.*, **2003,** *37*, 2497-2505.

Yoshida, T. Estimation of absorption of aromatic hydrocarbons diffusing from interior materials in automobile cabins by inhalation toxicokinetic analysis in rats. *J. Appl. Toxicol.*, **2010,** *30*, 525-532.

Yoshida, T. and Matsunaga, I. A case study on identification of airborne organic compounds and time courses of their concentrations in the cabin of a new car for private use. *Environ. Int.*, **2006a,** *32*, 58-79.

Yoshida, T.; Matsunaga, I.; Tomioka, K.; Kumagai, S. Interior Air Pollution in Automotive Cabins by Volatile Organic Compounds Diffusing from Interior Materials: I. Survey of 101 Types of Japanese Domestically Produced Cars for Private Use. *Indoor Built Environ.*, **2006b,** *15*, 425-444.

Zanis, P. *In-situ* photochemical control of ozone at the Jungfraujoch in the Swiss Alps, *Ph.D. Thesis*, University of Berne Switzerland, 1999.